

# A constrained gentlest ascent dynamics and its applications to finding excited states of Bose–Einstein condensates

Wei Liu<sup>a,b</sup>, Ziqing Xie<sup>a</sup>, Yongjun Yuan<sup>a,\*</sup>

<sup>a</sup>*Key Laboratory of Computing and Stochastic Mathematics (Ministry of Education), School of Mathematics and Statistics, Hunan Normal University, Changsha, Hunan 410081, PR China*

<sup>b</sup>*Present address: South China Research Center for Applied Mathematics and Interdisciplinary Studies, South China Normal University, Guangzhou 510631, PR China*

---

## Abstract

In this paper, the gentlest ascent dynamics (GAD) developed in W. E and X. Zhou (2011) [21] is extended to a constrained gentlest ascent dynamics (CGAD) to find constrained saddle points with any specified Morse indices. It is proved that the linearly stable steady state of the proposed CGAD is exactly a nondegenerate constrained saddle point with a corresponding Morse index. Meanwhile, the locally exponential convergence of an idealized CGAD near nondegenerate constrained saddle points with corresponding indices is also verified. The CGAD is then applied to find excited states of single-component Bose–Einstein condensates (BECs) in the order of their Morse indices via computing constrained saddle points of the corresponding Gross–Pitaevskii energy functional under the normalization constraint. In addition, properties of the excited states of BECs in the linear/nonlinear cases are mathematically/numerically studied. Extensive numerical results are reported to show the effectiveness and robustness of our method and demonstrate some interesting physics.

*Keywords:* constrained saddle points, constrained gentlest ascent dynamics, linear stability, Bose–Einstein condensates, excited states

---

## 1. Introduction

Saddle points appear widely in various scientific fields as, for example, excited states in atomic, molecular and optical systems or transition states in chemical reactions. Particularly, the index-1 saddle point is a central concept in the study of rare events, which corresponds to the transition state between metastable states in randomly perturbed system [20, 21]. In practice, excited states in some scenarios only occur instantaneously. And, transition states usually occur with very low probability. Owing to these difficulties in direct experimental observation, the effective numerical search of saddle points has attracted more and more attentions. Different numerical algorithms for finding saddle points have been carried out in the literature in recent decades, most of which are related to unconstrained saddle points. However, many physical/chemical/biological systems in practical scientific problems are constrained by one or more physical constraints, e.g., the wave function of a Bose–Einstein condensate (BEC) is constrained by one or more normalization conditions [15, 3]. And, the volume and surface area of a biological vesicle membrane are fixed to be prescribed constants in the phase field model [18, 13]. This motivates us to concern finding constrained saddle points.

---

\*Corresponding author.

*Email addresses:* wliu@m.scnu.edu.cn (Wei Liu), ziqingxie@hunnu.edu.cn (Ziqing Xie), yuanyongjun0301@163.com (Yongjun Yuan)

In terms of numerical methods for finding unconstrained saddle points of given nonconvex energy functionals or multiple unstable solutions of nonlinear partial differential equations, we refer to the mountain-pass algorithm [14], the high-linking algorithm [17], the local minimax method (LMM) [30], the search extension method [11], the bifurcation method [37], the string method [20], the gentlest ascent dynamics (GAD) [21], the dimer method [26] and the shrinking dimer dynamics (SDD) [44], etc. Typically, the GAD developed by E and Zhou [21] is a continuous dynamical system that describes the escape from the attractive basins of stable invariant sets. It is proved that the linearly stable steady state of the GAD proposed in [21] is exactly an index-1 saddle point. And, due to its simplicity and effectiveness, the GAD has been applied to compute index-1 saddle points in many problems [29, 28, 45]. Several variants of the GAD such as the iterative minimization algorithm [22] and the multiscale GAD [24], were presented in literature. In [35], Quapp and Bofill proposed a generalized GAD algorithm that can compute unconstrained high-index saddle points. In addition, the SDD proposed by Zhang and Du [43] is closely related to the GAD. In fact, the SDD can be obtained by approximating the Hessian in the formulation of the GAD with first-order derivatives and introducing an additional dynamics for shrinking the length of the so-called dimer. Recently, Yin, Zhang and Zhang [41] extended the SDD to find unconstrained high-index saddle points, and proposed a high-index optimization-based shrinking dimer (HiOSD) method.

There have existed several effective numerical methods in the literature to find constrained saddle points. In [19], Zhang and Du proposed a constrained string method to compute the minimum energy path (MEP) with given constraints. In this way, the index-1 constrained saddle point given by the local maximizer of the energy functional on the MEP can be obtained accordingly. In a subsequent work of [44], Zhang and Du also proposed a constrained SDD (CSDD) [43] to search index-1 constrained saddle points. In [28], Li, Lu and Yang modified the GAD to find index-1 saddle points of the Kohn–Sham density functional under the orthonormality constraints. Other numerical methods for finding constrained saddle points include the LMM based on the Rayleigh quotient or the active Lagrangian [39, 40], the LMM using virtual geometric objects [31], and the Ljusternik–Schnirelman minimax algorithm [38]. These methods can be regarded as the variants of the original LMM developed by Li and Zhou in [30] and corresponding two-level optimization problems have to be solved. In summary, the above mentioned methods are mainly used to compute index-1 constrained saddle points or their efficiency are needed to be further improved. Thus, efficient numerical methods as well as the corresponding theoretical analysis are still called for to compute the general high-index constrained saddle points.

One of the important applications of computing constrained saddle points is to find the excited states of BECs. The BEC was first realized experimentally in dilute weakly interacting gases in 1995 [1, 8, 16]. As is known, one of the basic problems in numerical studies of BEC is to determine the stationary states, i.e., the critical points of the energy functional under certain normalization constraints, by the mean field Gross–Pitaevskii (GP) theory. In the physics literatures, the stationary state with the lowest energy is called the ground state of BEC, whereas the stationary states with higher energies are usually called excited states. In the past two decades, based on the Gross–Pitaevskii equations (GPEs), many effective numerical methods for computing the ground states of BECs have been developed, as reviewed in, e.g., [3]. However, the numerical methods for finding excited states of BECs are still relatively limited. The normalized gradient flow or the imaginary time evolution method [5], as one of the most popular techniques for computing the ground states of BECs, has been extended to compute the ‘first’ excited states of single-component BECs with symmetries, see, e.g., [5, 2]. In addition, some continuation algorithms [10, 12] and Newton-based iterative algorithm [36] are also designed to compute excited states of BECs. However, the convergence of these methods depend on the choice of initial data, and more efficient and accurate methods to compute excited states of BECs are still worthwhile explored.

In this paper, we are interested in developing a continuous dynamical system to stably search for constrained saddle points with any specified Morse indices. Due to the difficulties caused by

constraints, instability, nonlinearity and nonconvexity, it is quite challenging to find constrained saddle points with general constraints in a stable way, especially for high-index ones. Inspired by the works of the original GAD [21] for index-1 unconstrained saddle points and the CSDD [43] for index-1 constrained saddle points, we are aimed to propose a constrained gentlest ascent dynamics (CGAD) to compute general constrained saddle points with any specified indices and analyze its linear stability and local convergence. Further, we apply the CGAD to simulate excited states of BECs to demonstrate its effectiveness and robustness and then illustrate an interesting problem, i.e., the relation among the GP energies, chemical potentials and Morse indices of the excited states (as constrained saddle points) of BECs. In fact, it was found numerically that both the GP energy and chemical potential of the excited state increase with the increase of its Morse index, whereas the excited states with the same index may be at different energy levels.

The paper is organized as follows. In section 2, we describe the definitions of constrained saddle points and their Morse indices. In section 3, we briefly review the original GAD and construct the CGAD to search for index- $k$  constrained saddle points. In section 4, the mathematical justifications of the CGAD, including the linear stability and the local convergence of an idealized CGAD, are analyzed. In section 5, the CGAD is implemented to find some excited states of single-component BECs. Several interesting mathematical properties of excited states and the detailed numerical results in 1D and 2D are presented. Finally, some conclusions are drawn in section 6.

## 2. Constrained saddle points and Morse indices

Let  $X$  be a real Hilbert space with its inner product  $\langle \cdot, \cdot \rangle$  and norm  $\| \cdot \|$ . An energy functional  $E \in C^2(X, \mathbb{R})$  and  $m$  constraint functionals  $G_i \in C^2(X, \mathbb{R})$ ,  $i = 1, 2, \dots, m$  are given. Consider critical points of the energy functional  $E$  under constraints

$$G_i(u) = 0, \quad i = 1, 2, \dots, m. \quad (2.1)$$

Denote  $\mathcal{M} = \{u \in X : G_i(u) = 0, i = 1, 2, \dots, m\}$  as the constraint manifold.

**Definition 2.1.**  $u^* \in X$  is called a constrained critical point of  $E$  on the manifold  $\mathcal{M}$ , or a constrained critical point of  $E$  under the constraints (2.1), if there exist  $\mu_i^* \in \mathbb{R}$ ,  $i = 1, 2, \dots, m$ , such that

$$E'(u^*) - \sum_{i=1}^m \mu_i^* G_i'(u^*) = 0, \quad G_i(u^*) = 0, \quad i = 1, 2, \dots, m, \quad (2.2)$$

where  $E'$  and  $G_i'$  represent the Fréchet derivatives (or gradients) of  $E$  and  $G_i$ , respectively. The constrained critical point that is not local extremizer (i.e., maximizer or minimizer) is called a constrained saddle point.

Throughout this paper, we assume that the constraints (2.1) are *regular*, i.e., their gradients  $G_i'(u)$ ,  $i = 1, 2, \dots, m$ , are linearly independent for all  $u \in \mathcal{M}$ . Then  $\mathcal{M}$  is a  $C^2$  differential manifold, and its tangent space at  $u \in \mathcal{M}$  is given by  $T_u\mathcal{M} = \{v \in X : \langle G_i'(u), v \rangle = 0, i = 1, 2, \dots, m\}$ . A direct computation shows that the orthogonal projection operator from  $X$  onto the tangent space  $T_u\mathcal{M}$  at  $u \in \mathcal{M}$  takes

$$P_u = I - \sum_{i=1}^m \sum_{j=1}^m g_{ij}(u) [G_i'(u) \otimes G_j'(u)], \quad (2.3)$$

where  $I$  is the identity operator,  $g_{ij}(u)$  are the  $(i, j)$ -elements of the inverse to the (positive definite) Gram matrix  $[\langle G_i'(u), G_j'(u) \rangle]_{i,j=1,2,\dots,m}$ , and  $\otimes$  denotes the tensor product operator defined as  $(v \otimes w)\xi = \langle w, \xi \rangle v$ ,  $\forall v, w, \xi \in X$ . The projected gradient of  $E$  at  $u \in \mathcal{M}$  can be written as

$$F(u) := P_u E'(u) = E'(u) - \sum_{i=1}^m \mu_i(u) G_i'(u), \quad (2.4)$$

with  $\mu_i(u) = \sum_{j=1}^m g_{ij}(u) \langle G'_j(u), E'(u) \rangle$ ,  $i = 1, 2, \dots, m$ . Clearly,  $u^* \in X$  is a constrained critical point of  $E$  on  $\mathcal{M}$  if and only if  $G_i(u^*) = 0$ ,  $i = 1, 2, \dots, m$ , and  $F(u^*) = 0$ .

For  $u \in \mathcal{M}$ , denoting  $H(u) := E''(u) - \sum_{i=1}^m \mu_i(u) G''_i(u)$  the effective Hessian operator [34], we define the projected Hessian operator

$$\hat{H}(u) = P_u H(u) P_u : T_u \mathcal{M} \rightarrow T_u \mathcal{M}, \quad (2.5)$$

which is a self-adjoint linear operator on the tangent space  $T_u \mathcal{M}$ . Similar to the concept of Morse indices for unconstrained critical points [9], the stability/instability of a constrained critical point  $u \in \mathcal{M}$  can be depicted by examining the spectrum of the linear operator  $\hat{H}(u)$ . More precisely, we introduce the following definition.

**Definition 2.2.** Assume that  $u^*$  is a constrained critical point of  $E$  on the manifold  $\mathcal{M}$ . Let  $T_{u^*} \mathcal{M} = T^- \oplus T^0 \oplus T^+$ ,  $\dim(T^0) < \infty$ , where  $T^-$ ,  $T^0$  and  $T^+$  are, respectively, the maximum negative, null, and maximum positive subspaces according to the spectral decomposition of the linear operator  $\hat{H}(u^*) : T_{u^*} \mathcal{M} \rightarrow T_{u^*} \mathcal{M}$ . The Morse index of  $u^*$  is defined as  $\text{index}(u^*) = \dim(T^-)$ .  $u^*$  is nondegenerate if  $T^0 = \{0\}$ . Otherwise,  $u^*$  is degenerate and  $\dim(T^0)$  is called its nullity. When  $\text{index}(u^*) = k$  ( $k = 1, 2, \dots$ ),  $u^*$  is called an index- $k$  constrained saddle point,  $T^-$  is called its unstable (tangent) subspace and each nonzero vector in  $T^-$  is called an unstable (tangent) direction at  $u^*$ .

### 3. The constrained gentlest ascent dynamics

#### 3.1. Review of the GAD

To propose our CGAD method, we first review the GAD developed in [21] for finding index-1 unconstrained saddle points of  $E$ , which is formulated as

$$\begin{cases} \dot{u} = -E'(u) + 2\langle E'(u), v \rangle v, \\ \dot{v} = -E''(u)v + \langle E''(u)v, v \rangle v, \end{cases} \quad (3.1)$$

starting at  $(u(0), v(0)) = (u_0, v_0) \in X^2$  with  $v_0$  satisfying the normalization condition  $\|v_0\| = 1$ . Compared to the steepest descent dynamics or gradient flow

$$\dot{u} = -E'(u), \quad (3.2)$$

which works for finding local minima, the GAD (3.1) consists of two equations. The first equation in (3.1) can be obtained by performing the Householder transformation for the gradient flow with respect to the auxiliary unit vector  $v$ , where the last term in it makes  $v$  a stable direction. The second equation in (3.1), evolving the vector  $v$ , is constructed by solving the Rayleigh quotient minimization problem  $\min_{\|v\|=1} \langle E''(u)v, v \rangle$ , which makes  $v$  approximate the unstable direction of the target index-1 saddle point. It was proved in [21] that, for an appropriately smooth energy function  $E$  defined on an Euclidean space, the linearly stable steady state of the GAD (3.1) is exactly an index-1 saddle point of  $E$ .

#### 3.2. CGAD for index-1 constrained saddle points

The aim of this section is to propose the CGAD for finding constrained saddle points with any specified indices. To clarify the idea, we first construct the formulation of the CGAD to search for index-1 constrained saddle points.

Let  $u \in \mathcal{M}$  be an approximation of an index-1 constrained saddle point of  $E$  on the constraint manifold  $\mathcal{M} = \{u \in X : G_i(u) = 0, i = 1, 2, \dots, m\}$ , and the unit vector  $v \in T_u \mathcal{M}$  be an approximation of the corresponding unstable tangent direction, see Fig. 1 (left). We discuss below how to construct the evolution equations of  $u$  and  $v$ .

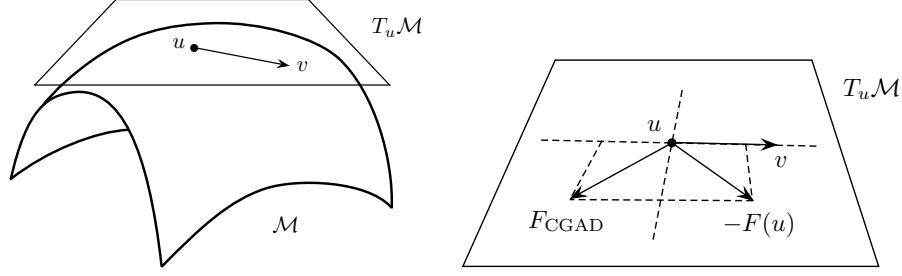


Figure 1: Illustration of the index-1 CGAD. Left:  $u \in \mathcal{M}$  and  $v \in T_u \mathcal{M}$  approximate an index-1 constrained saddle point on the manifold  $\mathcal{M}$  and its unit unstable direction, respectively. Right: the projected gradient  $F(u) = P_u E'(u)$  has the decomposition  $F(u) = F_v(u) + F_\perp(u)$  with  $F_v(u) \in T_u \mathcal{M} \cap \text{span}\{v\}$  and  $F_\perp(u) \in T_u \mathcal{M} \cap \text{span}\{v\}^\perp$ , and thus, the force of the index-1 CGAD to evolve  $u$  is constructed as  $F_{\text{CGAD}} = F_v(u) - F_\perp(u) = -F(u) + 2F_v(u)$ .

- **Construction of the dynamics for  $u$ .** To guarantee that  $u$  moves towards an index-1 constrained saddle point, the evolution of  $u$  in the direction  $v$  has to increase the energy, while the evolution in other directions decreases the energy. Moreover, to preserve the constraint  $u \in \mathcal{M}$  (i.e.,  $G_i(u) = 0$ ,  $i = 1, 2, \dots, m$ ), the force to evolve  $u$  must be in the tangent space  $T_u \mathcal{M}$ . Thus, we construct the dynamics for  $u$  as

$$\dot{u} = F_v(u) - F_\perp(u), \quad (3.3)$$

where  $F_v(u) = \langle F(u), v \rangle v$  is the component of the projected gradient  $F(u) = P_u E'(u)$  in  $v$  and  $F_\perp(u) = F(u) - \langle F(u), v \rangle v$  the component of  $F(u)$  in the orthogonal complement of  $v$ , as illustrated in Fig. 1 (right). Intuitively, the first term in (3.3) makes the energy increase in  $v$  and the second term makes the energy decrease in other directions.

- **Construction of the dynamics for  $v$ .** From the definition of unstable directions, if  $u$  is an index-1 constrained saddle point, its unstable direction  $v$  is an eigenvector of the projected Hessian  $\hat{H}(u)$  corresponding to the unique negative eigenvalue. By the Rayleigh-Ritz variational principle [42],  $v$  can be obtained by solving the following minimization problem

$$\min_{v \in T_u \mathcal{M}, \|v\|^2=1} \langle \hat{H}(u)v, v \rangle. \quad (3.4)$$

Considering the Lagrangian

$$\mathcal{L}(v, \lambda, \bar{\lambda}_1, \bar{\lambda}_2, \dots, \bar{\lambda}_m) = \frac{1}{2} \langle \hat{H}(u)v, v \rangle - \frac{\lambda}{2} (\|v\|^2 - 1) - \sum_{i=1}^m \bar{\lambda}_i \langle G'_i(u), v \rangle, \quad (3.5)$$

we construct the dynamics for  $v$  as

$$\dot{v} = -\frac{\delta}{\delta v} \mathcal{L}(v, \lambda, \bar{\lambda}_1, \bar{\lambda}_2, \dots, \bar{\lambda}_m) = -\hat{H}(u)v + \lambda v + \sum_{i=1}^m \bar{\lambda}_i G'_i(u), \quad (3.6)$$

where  $\lambda = \lambda(u, v)$  and  $\bar{\lambda}_i = \bar{\lambda}_i(u, v)$  are the Lagrange multipliers corresponding to the constraints  $\|v\|^2 = 1$  and  $\langle G'_i(u), v \rangle = 0$ ,  $i = 1, 2, \dots, m$  (i.e.,  $v \in T_u \mathcal{M}$ ), respectively.

In summary, the CGAD for finding an index-1 constrained saddle point is formulated as

$$\begin{cases} \dot{u} = -F(u) + 2\langle F(u), v \rangle v, \\ \dot{v} = -\hat{H}(u)v + \lambda v + \sum_{i=1}^m \bar{\lambda}_i G'_i(u), \end{cases} \quad (3.7)$$

with the initial data  $(u(0), v(0)) = (u_0, v_0)$  satisfying  $u_0 \in \mathcal{M}$ ,  $v_0 \in T_{u_0}\mathcal{M}$  and  $\|v_0\|^2 = 1$ . The Lagrange multipliers  $\lambda$  and  $\bar{\lambda}_i$  ( $i = 1, 2, \dots, m$ ) in (3.7) are chosen such that the flow preserves the constraints  $\|v\|^2 = 1$  and  $\langle G'_i(u), v \rangle = 0$  ( $i = 1, 2, \dots, m$ ), respectively. Therefore,  $\langle v, \dot{v} \rangle = 0$  and  $\langle G'_i(u), \dot{v} \rangle + \langle G''_i(u)\dot{u}, v \rangle = 0$ , which lead to

$$\lambda = \langle \hat{H}(u)v, v \rangle, \quad \bar{\lambda}_i = \sum_{j=1}^m g_{ij}(u) \langle G''_j(u)v, F(u) - 2\langle F(u), v \rangle v \rangle, \quad i = 1, 2, \dots, m.$$

### 3.3. CGAD for high-index constrained saddle points

Now, we extend the index-1 CGAD (3.7) to general high-index cases. To construct the CGAD for finding an index- $k$  ( $k = 1, 2, 3, \dots$ ) constrained saddle point of the energy functional  $E \in C^2(X, \mathbb{R})$  on the constraint manifold  $\mathcal{M}$ , we need to consider  $k$  linearly independent unstable tangent directions  $v_1, v_2, \dots, v_k \in T_u\mathcal{M}$  (see Fig. 2). Let  $u \in \mathcal{M}$  be an approximation of an index- $k$  constrained saddle point and  $V = \text{span}\{v_1, v_2, \dots, v_k\}$  the approximation of corresponding unstable subspace. Denote  $W$  by the orthogonal complement of  $V$  in  $T_u\mathcal{M}$ .

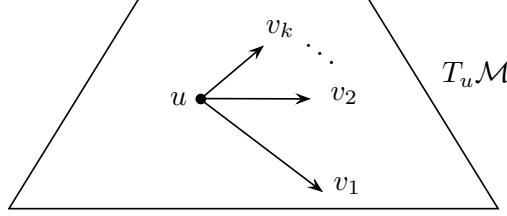


Figure 2: Illustration of unstable directions  $v_1, v_2, \dots, v_k \in T_u\mathcal{M}$  for an index- $k$  constrained saddle point  $u \in \mathcal{M}$ .

In order to make  $u$  move towards an index- $k$  constrained saddle point, the force that evolves  $u$  needs to be in the tangent space  $T_u\mathcal{M}$  with its components in  $V$  and  $W$  increasing and decreasing the energy, respectively. It is natural to evolve  $u$  by the steepest ascent dynamics in  $V$  and the steepest descent dynamics in  $W$ , i.e., the dynamics for  $u$  is as

$$\dot{u} = F_V(u) - F_W(u), \quad (3.8)$$

where  $F_V(u)$  and  $F_W(u) = F(u) - F_V(u)$  are the orthogonal projections of the projected gradient  $F(u) = P_u E'(u)$  on  $V$  and  $W$ , respectively. If  $v_1, v_2, \dots, v_k \in T_u\mathcal{M}$  satisfy the orthonormal conditions:  $\langle v_i, v_j \rangle = \delta_{ij}$ , then  $F_V(u) = \sum_{j=1}^k \langle F(u), v_j \rangle v_j$ , and (3.8) becomes

$$\dot{u} = -F(u) + 2F_V(u) = -F(u) + 2 \sum_{j=1}^k \langle F(u), v_j \rangle v_j. \quad (3.9)$$

It is worthwhile to point out that, if  $u$  is an index- $k$  constrained saddle point, its unstable directions  $v_1, v_2, \dots, v_k$  can be taken as the orthonormal eigenvectors of the projected Hessian  $\hat{H}(u)$  corresponding to the  $k$  smallest and negative eigenvalues. By the Rayleigh-Ritz variational principle [42], the eigenvector  $v_1$  corresponding to the smallest eigenvalue can be obtained by minimizing  $\langle \hat{H}(u)v_1, v_1 \rangle$  under the constraints  $v_1 \in T_u\mathcal{M}$  and  $\|v_1\|^2 = 1$ . And, when eigenvectors  $v_1, v_2, \dots, v_{i-1}$  of  $\hat{H}(u)$  corresponding to the first  $i-1$  smallest eigenvalues are known, the eigenvector  $v_i$  corresponding to the  $i$ -th smallest eigenvalue can be obtained by solving the following Rayleigh-Ritz minimization problem [42]

$$\min_{v_i} \langle \hat{H}(u)v_i, v_i \rangle \quad \text{s.t.} \quad v_i \in T_u\mathcal{M}, \quad \langle v_i, v_j \rangle = \delta_{ij}, \quad j = 1, 2, \dots, i. \quad (3.10)$$

Consider the Lagrangian

$$\begin{aligned} \mathcal{L}_i(v_i, \lambda_{i1}, \lambda_{i2}, \dots, \lambda_{ii}, \bar{\lambda}_{i1}, \bar{\lambda}_{i2}, \dots, \bar{\lambda}_{im}) \\ = \frac{1}{2} \langle \hat{H}(u)v_i, v_i \rangle - \frac{\lambda_{ii}}{2} (\|v_i\|^2 - 1) - \sum_{j=1}^{i-1} \lambda_{ij} \langle v_i, v_j \rangle - \sum_{l=1}^m \bar{\lambda}_{il} \langle G'_l(u), v_i \rangle, \end{aligned}$$

with Lagrange multipliers  $\lambda_{ij}$  ( $j = 1, 2, \dots, i$ ) and  $\bar{\lambda}_{il}$  ( $l = 1, 2, \dots, m$ ) corresponding to constraints  $\langle v_i, v_j \rangle = \delta_{ij}$  and  $\langle G'_l(u), v_i \rangle = 0$  (i.e.,  $v_i \in T_u \mathcal{M}$ ), respectively. The gradient flow for solving (3.10) is given by the following dynamics for  $v_i$  ( $i = 1, 2, \dots, k$ ):

$$\dot{v}_i = -\frac{\delta \mathcal{L}_i}{\delta v_i} = -\hat{H}(u)v_i + \sum_{j=1}^i \lambda_{ij} v_j + \sum_{l=1}^m \bar{\lambda}_{il} G'_l(u).$$

Based on the above discussion, we propose the following CGAD to search for the index- $k$  constrained saddle point:

$$\begin{cases} \gamma_0 \dot{u} = -F(u) + 2 \sum_{i=1}^k \langle F(u), v_i \rangle v_i, \\ \gamma_i \dot{v}_i = -\hat{H}(u)v_i + \sum_{j=1}^i \lambda_{ij} v_j + \sum_{l=1}^m \bar{\lambda}_{il} G'_l(u), \quad i = 1, 2, \dots, k. \end{cases} \quad (3.11)$$

Here  $\gamma_i > 0$  ( $i = 0, 1, \dots, k$ ) are relaxation parameters. The Lagrange multipliers  $\lambda_{ij}$  ( $j = 1, 2, \dots, i$ ) and  $\bar{\lambda}_{il}$  ( $l = 1, 2, \dots, m$ ) are chosen such that the flow preserves the constraints  $\langle v_i, v_j \rangle = \delta_{ij}$  and  $\langle G'_l(u), v_i \rangle = 0$ , respectively, which leads to  $\langle \dot{v}_i, v_j \rangle + \langle v_i, \dot{v}_j \rangle = 0$  and  $\langle G''_l(u)\dot{u}, v_i \rangle + \langle G'_l(u), \dot{v}_i \rangle = 0$ . Hence

$$\lambda_{ij} = (1 + \gamma_i/\gamma_j - \delta_{ij}) \langle \hat{H}(u)v_i, v_j \rangle, \quad j = 1, 2, \dots, i, \quad (3.12)$$

$$\bar{\lambda}_{il} = \frac{\gamma_i}{\gamma_0} \sum_{l'=1}^m g_{ll'}(u) \left\langle G''_{l'}(u)v_i, F(u) - 2 \sum_{j=1}^k \langle F(u), v_j \rangle v_j \right\rangle, \quad l = 1, 2, \dots, m, \quad (3.13)$$

for  $i = 1, 2, \dots, k$ . The initial data  $(u(0), v_1(0), \dots, v_k(0))$  of (3.11) is assumed to satisfy  $u(0) \in \mathcal{M}$ ,  $v_i(0) \in T_{u(0)} \mathcal{M}$  and  $\langle v_i(0), v_j(0) \rangle = \delta_{ij}$  for  $1 \leq j \leq i \leq k$ , or equivalently,

$$G_l(u(0)) = 0, \quad l = 1, 2, \dots, m, \quad (3.14a)$$

$$\langle G'_l(u(0)), v_i(0) \rangle = 0, \quad l = 1, 2, \dots, m, \quad i = 1, 2, \dots, k, \quad (3.14b)$$

$$\langle v_i(0), v_j(0) \rangle = \delta_{ij}, \quad 1 \leq j \leq i \leq k. \quad (3.14c)$$

Clearly, the index-1 CGAD (3.7) is a special case of the CGAD (3.11).

**Remark 3.1.** According to the CGAD (3.11), the CSDD proposed in [43] for finding index-1 constrained saddle points can be easily extended to a high-index CSDD for searching for index- $k$  constrained saddle points. Actually, the approximation

$$\hat{H}(u)v_i \approx \frac{F(u + \ell v_i) - F(u - \ell v_i)}{2\ell}, \quad i = 1, 2, \dots, k,$$

and an additional dynamics for shrinking the parameter  $\ell > 0$ , e.g.,  $\dot{\ell} = -\ell$  [43, 44], should be implemented to construct the index- $k$  CSDD from the CGAD (3.11).

The following lemma states that the CGAD (3.11) preserves exactly the constraints (3.14).

**Lemma 3.2.** Assume that  $E, G_l \in C^2$ ,  $l = 1, 2, \dots, m$ , and the constraints (2.1) are regular. Let  $(u(t), v_1(t), \dots, v_k(t))$  be the solution of (3.11) with the initial data satisfying (3.14). Then

$$G_l(u(t)) \equiv 0, \quad l = 1, 2, \dots, m, \quad (3.15a)$$

$$\langle G'_l(u(t)), v_i(t) \rangle \equiv 0, \quad l = 1, 2, \dots, m, \quad i = 1, 2, \dots, k, \quad (3.15b)$$

$$\langle v_i(t), v_j(t) \rangle \equiv \delta_{ij}, \quad 1 \leq j \leq i \leq k. \quad (3.15c)$$

*Proof.* See detailed proof in Appendix A. □

#### 4. Linear stability and local convergence

In this section, we study the stability and convergence of the CGAD (3.11). The following lemma will play important role in the subsequent analysis, with its proof detailed in Appendix B.

**Lemma 4.1.** Assume that  $E, G_i \in C^2$ ,  $i = 1, 2, \dots, m$ , and the constraints (2.1) are regular. Then, for  $u \in \mathcal{M}$ ,

$$F'(u)v = \hat{H}(u)v - \sum_{i=1}^m \sum_{j=1}^m g_{ij}(u) \langle G''_j(u)F(u), v \rangle G'_i(u), \quad \forall v \in T_u\mathcal{M}. \quad (4.1)$$

In particular,  $F'(u^*) = \hat{H}(u^*)$  if  $u^* \in \mathcal{M}$  is a constrained critical point.

##### 4.1. Linear stability of the CGAD

We now show that the linearly stable steady state of the CGAD (3.11) is exactly a nondegenerate index- $k$  constrained saddle point of  $E$  on the manifold  $\mathcal{M}$ . Similar results of the GAD for unconstrained saddle points and the CSDD for index-1 constrained saddle point can be found in [21, 41] and [43], respectively.

**Theorem 4.2.** Assume that  $E, G_l \in C^3$ ,  $l = 1, 2, \dots, m$ , and the constraints (2.1) are regular. Let  $u^* \in \mathcal{M}$  and  $v_i^* \in T_{u^*}\mathcal{M}$ ,  $i = 1, 2, \dots, k$ , satisfy  $\langle v_i^*, v_j^* \rangle = \delta_{ij}$ .

(a)  $(u^*, v_1^*, \dots, v_k^*)$  is a steady state of (3.11) if and only if  $u^*$  is a constrained critical point of  $E$  on the manifold  $\mathcal{M}$  and  $v_i^*$ ,  $i = 1, 2, \dots, k$ , are eigenvectors of  $\hat{H}(u^*)$ .

(b)  $(u^*, v_1^*, \dots, v_k^*)$  is a linearly stable steady state of (3.11) if and only if the following hold:

- (i)  $u^*$  is a nondegenerate index- $k$  constrained saddle point of  $E$  on the manifold  $\mathcal{M}$ ;
- (ii) all the eigenvalues of  $\hat{H}(u^*)$ , say  $\{\lambda_i^*\}$ , satisfy  $\lambda_1^* < \lambda_2^* < \dots < \lambda_k^* < 0 < \lambda_{k+1}^* \leq \lambda_{k+2}^* \leq \dots$ ;
- (iii) for  $i = 1, 2, \dots, k$ ,  $v_i^*$  is the eigenvector of  $\hat{H}(u^*)$  corresponding to the eigenvalue  $\lambda_i^*$ .

*Proof.* (a) *Necessity.* Suppose that  $(u^*, v_1^*, \dots, v_k^*)$  is a steady state of (3.11), i.e.,

$$-F(u^*) + 2 \sum_{i=1}^k \langle F(u^*), v_i^* \rangle v_i^* = 0, \quad (4.2)$$

$$-\hat{H}(u^*)v_i^* + \sum_{j=1}^i \lambda_{ij}^* v_j^* + \sum_{l=1}^m \bar{\lambda}_{il}^* G'_l(u^*) = 0, \quad i = 1, 2, \dots, k, \quad (4.3)$$

where  $\lambda_{ij}^*$  and  $\bar{\lambda}_{il}^*$  are given in (3.12)-(3.13) with  $(u, v_1, \dots, v_k)$  replaced by  $(u^*, v_1^*, \dots, v_k^*)$ . Noting that  $\langle v_i^*, v_j^* \rangle = \delta_{ij}$ , taking the inner product in both sides of (4.2) with  $v_j^*$  yields  $\langle F(u^*), v_j^* \rangle = 0$ ,



$j = 1, 2, \dots, k$ . Therefore,  $F(u^*) = 0$ , i.e.,  $u^*$  is a constrained critical point. Moreover, by (3.13), we have  $\bar{\lambda}_{il}^* = 0$ , thus (4.3) becomes

$$\hat{H}(u^*)v_i^* = \sum_{j=1}^i \lambda_{ij}^* v_j^*, \quad i = 1, 2, \dots, k. \quad (4.4)$$

Taking the inner product in both side of (4.4) with  $v_l^*$  ( $\forall l < i$ ) implies that  $\langle \hat{H}(u^*)v_i^*, v_l^* \rangle = \sum_{j=1}^i \lambda_{ij}^* \langle v_j^*, v_l^* \rangle = \lambda_{il}^*$ , which states  $\lambda_{il}^* = 0$  (otherwise, one gets a contradiction with (3.12)). Consequently,  $\hat{H}(u^*)v_i^* = \lambda_{ii}^* v_i^*$ ,  $i = 1, 2, \dots, k$ , i.e.,  $\{(\lambda_{ii}^*, v_i^*)\}_{i=1}^k$  are eigenpairs of  $\hat{H}(u^*)$ .

*Sufficiency.* Suppose that  $u^*$  is a constrained critical point of  $E$  on the manifold  $\mathcal{M}$  and  $v_i^*$  ( $i = 1, 2, \dots, k$ ) are eigenvectors of  $\hat{H}(u^*)$ . Then  $F(u^*) = 0$ , (4.2) is satisfied, and  $\bar{\lambda}_{il}^* = 0$ . On the other hand, for each  $i = 1, 2, \dots, k$ , since  $v_i^*$  is an eigenvector of  $\hat{H}(u^*)$ , there exists an  $\omega_i^* \in \mathbb{R}$  such that  $\hat{H}(u^*)v_i^* = \omega_i^* v_i^*$ . We have

$$\lambda_{ij}^* = (1 + \gamma_i/\gamma_j - \delta_{ij}) \langle \hat{H}(u^*)v_i^*, v_j^* \rangle = (1 + \gamma_i/\gamma_j - \delta_{ij}) \omega_i^* \delta_{ij} = \omega_i^* \delta_{ij}.$$

Thus, (4.3) holds. Consequently,  $(u^*, v_1^*, \dots, v_k^*)$  is a steady state of (3.11).

(b) Consider the Jacobian operator of the right-hand-side of (3.11), denoted by  $J$ . Direct computations and the application of Lemma 4.1 show that

$$J = \begin{pmatrix} J_{00} & J_{01} & J_{02} & \cdots & J_{0k} \\ J_{10} & J_{11} & 0 & \cdots & 0 \\ J_{20} & J_{21} & J_{22} & \cdots & 0 \\ \vdots & \vdots & \vdots & \ddots & \vdots \\ J_{k0} & J_{k1} & J_{k2} & \cdots & J_{kk} \end{pmatrix},$$

where

$$\begin{aligned} J_{00} &= \frac{\delta \dot{u}}{\delta u} = -\frac{1}{\gamma_0} \left( I - 2 \sum_{j=1}^k v_j \otimes v_j \right) \left( \hat{H}(u) - \sum_{l=1}^m \sum_{l'=1}^m g_{ll'}(u) [G'_l(u) \otimes F(u)] G'_{l'}(u) \right), \\ J_{0i} &= \frac{\delta \dot{u}}{\delta v_i} = \frac{2}{\gamma_0} \left( \langle F(u), v_i \rangle I + v_i \otimes F(u) \right), \\ J_{ii} &= \frac{\delta \dot{v}_i}{\delta v_i} = \frac{1}{\gamma_i} \left( -\hat{H}(u) + \lambda_{ii} I + \sum_{j=1}^i (1 + \gamma_i/\gamma_j) (v_j \otimes v_j) \hat{H}(u) + \sum_{l=1}^m G'_l(u) \otimes \frac{\delta \bar{\lambda}_{il}}{\delta v_i} \right), \end{aligned}$$

for  $i = 1, 2, \dots, k$ , with

$$\frac{\delta \bar{\lambda}_{il}}{\delta v_i} = \frac{\gamma_i}{\gamma_0} \sum_{l'=1}^m g_{ll'}(u) \left[ G'_{l'}(u) \left( I - 2 \sum_{j=1}^k v_j \otimes v_j \right) F(u) - 2 \left( \langle F(u), v_i \rangle I + v_i \otimes F(u) \right) G'_{l'}(u) v_i \right].$$

Since at the steady state  $(u^*, v_1^*, \dots, v_k^*)$ ,  $F(u^*) = 0$  and  $\hat{H}(u^*)v_i^* = \lambda_i^* v_i^*$  with  $\lambda_i^* := \lambda_{ii}^* = \langle \hat{H}(u^*)v_i^*, v_i^* \rangle$ ,  $i = 1, 2, \dots, k$ , the Jacobian  $J$  at  $(u^*, v_1^*, \dots, v_k^*)$  is a linear operator from  $(T_{u^*} \mathcal{M})^{k+1}$  to  $(T_{u^*} \mathcal{M})^{k+1}$  and takes a block lower triangular form with diagonal blocks

$$\begin{aligned} J_{00} &= \frac{1}{\gamma_0} \left( 2 \sum_{j=1}^k \lambda_j^* (v_j^* \otimes v_j^*) - \hat{H}(u^*) \right), \\ J_{ii} &= \frac{\lambda_i^* I - \hat{H}(u^*)}{\gamma_i} + \sum_{j=1}^i \left( \frac{1}{\gamma_i} + \frac{1}{\gamma_j} \right) \lambda_j^* (v_j^* \otimes v_j^*), \quad i = 1, 2, \dots, k. \end{aligned}$$

Moreover, since  $\{(\lambda_i^*, v_i^*)\}_{i=1}^k$  are eigenpairs of  $\hat{H}(u^*)$ , the diagonal blocks  $J_{00}, J_{11}, \dots, J_{kk}$  and  $\hat{H}(u^*)$  share the same eigenvectors  $v_i^*$  ( $i = 1, 2, \dots, k$ ). Let  $\lambda_{k+1}^* \leq \lambda_{k+2}^* \leq \dots$  be all other eigenvalues of  $\hat{H}(u^*)$  and  $v_{k+1}^*, v_{k+2}^*, \dots \in T_{u^*}\mathcal{M}$  be the corresponding eigenvectors. Due to  $\hat{H}(u^*)$  is self-adjoint and  $\{v_j^*\}_{j=1}^k$  is orthonormal, one may assume that  $\{v_j^*\}_{j \geq 1}$  is an orthonormal system. It is calculated that

$$J_{00}v_l^* = \frac{1}{\gamma_0} \left( 2 \sum_{j=1}^k \lambda_j^* \langle v_j^*, v_l^* \rangle v_j^* - \hat{H}(u^*)v_l^* \right) = \begin{cases} (\lambda_l^*/\gamma_0)v_l^*, & 1 \leq l \leq k, \\ -(\lambda_l^*/\gamma_0)v_l^*, & l > k, \end{cases}$$

$$J_{ii}v_l^* = \frac{\lambda_i^*v_l^* - \hat{H}(u^*)v_l^*}{\gamma_i} + \sum_{j=1}^i \left( \frac{1}{\gamma_i} + \frac{1}{\gamma_j} \right) \lambda_j^* \langle v_j^*, v_l^* \rangle v_j^* = \begin{cases} (\lambda_i^*/\gamma_i + \lambda_l^*/\gamma_l)v_l^*, & 1 \leq l \leq i, \\ ((\lambda_i^* - \lambda_l^*)/\gamma_i)v_l^*, & l > i. \end{cases}$$

Hence all eigenvalues of  $J$  are given as

$$\{\lambda_i^*/\gamma_0, -\lambda_l^*/\gamma_0, \lambda_i^*/\gamma_i + \lambda_r^*/\gamma_r, (\lambda_i^* - \lambda_s^*)/\gamma_i, \quad \forall 1 \leq r \leq i \leq k < l, s > i\}.$$

Thus,  $(u^*, v_1^*, \dots, v_k^*)$  is a linearly stable steady state of (3.11) if and only if all eigenvalues of  $J$  are negative, i.e.,  $\lambda_1^* < \lambda_2^* < \dots < \lambda_k^* < 0 < \lambda_{k+1}^* \leq \lambda_{k+2}^* \leq \dots$ . Equivalently, (i)  $u^*$  is a nondegenerate index- $k$  constrained saddle point; (ii) all eigenvalues of  $\hat{H}(u^*)$  satisfy  $\lambda_1^* < \lambda_2^* < \dots < \lambda_k^* < 0 < \lambda_{k+1}^* \leq \lambda_{k+2}^* \leq \dots$ ; and (iii)  $v_i^*$  is the eigenvector of  $\hat{H}(u^*)$  corresponding to  $\lambda_i^*$ ,  $i = 1, 2, \dots, k$ .  $\square$

**Remark 4.3.** For the index-1 case, the condition/conclusion (ii) in part (b) of Theorem 4.2 does not need to appear in the theorem since it is implied by the nondegeneracy in (i).

#### 4.2. Locally exponential convergence of an idealized CGAD

Due to the complexity of constraints and nonlinearities, there are some potential difficulties in directly analyzing the global convergence of the CGAD (3.11). For simplicity, based on a similar idea to the study on an idealized version of the original GAD in [27], we consider the following idealized CGAD:

$$\dot{u} = -F(u) + 2 \sum_{i=1}^k \langle F(u), v_i(u) \rangle v_i(u), \quad u(0) = u_0 \in \mathcal{M}, \quad (4.5)$$

where  $v_i(u) \in T_u\mathcal{M}$ , satisfying  $\langle v_i(u), v_j(u) \rangle = \delta_{ij}$ , are exact eigenvectors of the linear operator  $\hat{H}(u) : T_u\mathcal{M} \rightarrow T_u\mathcal{M}$  corresponding to the smallest  $k$  eigenvalues  $\lambda_1(u) \leq \lambda_2(u) \leq \dots \leq \lambda_k(u)$ .

Since  $\dot{u} \in T_u\mathcal{M}$  by (4.5), we have

$$\frac{d}{dt} G_l(u) = \langle G_l'(u), \dot{u} \rangle = 0, \quad l = 1, 2, \dots, m.$$

The initial condition  $u(0) = u_0 \in \mathcal{M}$  implies  $G_l(u(t)) \equiv 0$ ,  $l = 1, 2, \dots, m$ , i.e.,  $u(t) \in \mathcal{M}$ . Thus, the dynamics (4.5) preserves the constraints (2.1). Moreover, we have the following locally exponential convergence result of the dynamics (4.5) around a nondegenerate index- $k$  constrained saddle point.

**Theorem 4.4.** Assume that  $E, G_l \in C^3$ ,  $l = 1, 2, \dots, m$ , and the constraints (2.1) are regular. Let  $u = u(t)$  be the solution of the dynamics (4.5). Then

$$\frac{d}{dt} \|F(u)\|^2 \leq -2 \min\{-\lambda_k(u), \lambda_{k+1}(u)\} \|F(u)\|^2, \quad \forall t \geq 0, \quad (4.6)$$

where  $\lambda_{k+1}(u)$  is the  $(k+1)$ -th smallest eigenvalue of  $\hat{H}(u)$ . Further, if there exists a constant  $c > 0$  such that  $\lambda_k(u) \leq -c$  and  $\lambda_{k+1}(u) \geq c$  for all  $t \geq 0$ , then

$$\|F(u(t))\| \leq e^{-ct} \|F(u_0)\|. \quad (4.7)$$

*Proof.* Applying Lemma 4.1, and noting that  $F(u), v_i(u) \in T_u\mathcal{M}$ ,  $\hat{H}(u)v_i(u) = \lambda_i(u)v_i(u)$ ,  $i = 1, 2, \dots, k$ , we have

$$\begin{aligned}
\frac{d}{dt}\|F(u)\|^2 &= 2\langle F'(u)\dot{u}, F(u) \rangle \\
&= 2\langle \hat{H}(u)\dot{u}, F(u) \rangle - 2\sum_{i=1}^m \sum_{j=1}^m g_{ij}(u) \langle G_j''(u)F(u), \dot{u} \rangle \langle G_i'(u), F(u) \rangle \\
&= 2\left\langle \hat{H}(u) \left( -F(u) + 2\sum_{i=1}^k \langle F(u), v_i(u) \rangle v_i(u) \right), F(u) \right\rangle \\
&= -2\left\langle \left( \hat{H}(u) - 2\sum_{i=1}^k \lambda_i(u) [v_i(u) \otimes v_i(u)] \right) F(u), F(u) \right\rangle.
\end{aligned}$$

Clearly, the smallest eigenvalue of the linear operator  $A(u) : T_u\mathcal{M} \rightarrow T_u\mathcal{M}$ , with

$$A(u) := \hat{H}(u) - 2\sum_{i=1}^k \lambda_i(u) [v_i(u) \otimes v_i(u)],$$

is  $c_u := \min\{-\lambda_k(u), \lambda_{k+1}(u)\}$ . Thus,  $\langle A(u)\varphi, \varphi \rangle \geq c_u\|\varphi\|^2$  for all  $\varphi \in T_u\mathcal{M}$ , and

$$\frac{d}{dt}\|F(u)\|^2 = -2\langle A(u)F(u), F(u) \rangle \leq -2c_u\|F(u)\|^2.$$

This is (4.6). Further, when  $c_u \geq c$  for some constant  $c > 0$  and for all  $t \geq 0$ , (4.6) becomes  $\frac{d}{dt}\|F(u)\|^2 \leq -2c\|F(u)\|^2$ . Then the conclusion (4.7) follows from the Grönwall's inequality.  $\square$

**Remark 4.5.** *Under all assumptions of Theorem 4.4, if some additional assumptions on compactness (e.g., the constrained Palais–Smale condition [31]) are made, one can establish the existence of a nondegenerate index- $k$  constrained saddle point  $u_* \in \mathcal{M}$  such that, for any initial data  $u_0 \in \mathcal{M}$  near  $u_*$ , the solution  $u = u(t)$  of the dynamics (4.5) converges to  $u_*$  as  $t \rightarrow +\infty$  with exponential convergence rate:*

$$\begin{aligned}
\|u(t) - u_*\| &\leq \int_t^\infty \|\dot{u}(s)\| ds \\
&= \int_t^\infty \left\| F(u(s)) - 2\sum_{i=1}^k \langle F(u(s)), v_i(u(s)) \rangle v_i(u(s)) \right\| ds \\
&= \int_t^\infty \|F(u(s))\| ds \\
&\leq e^{-ct} \|F(u_0)\|/c.
\end{aligned}$$

## 5. Applications to finding excited states of single-component BECs

The CGAD can be applied to solve many scientific problems. In this section, we apply the CGAD (3.11) to find real-valued excited states of single-component BECs.

Within the mean-field theory, the GP energy functional of the wave function  $\phi = \phi(\mathbf{x})$  of a single-component BEC in  $d$  ( $d = 1, 2, 3$ ) dimension is given as [15, 3]

$$E(\phi) = \int_U \left( \frac{1}{2} |\nabla\phi|^2 + V(\mathbf{x})|\phi|^2 + \frac{\beta}{2} |\phi|^4 \right) d\mathbf{x}, \quad (5.1)$$

where  $U \subset \mathbb{R}^d$  is the spatial domain,  $V(\mathbf{x}) \geq 0$  is the real-valued trapping potential and the parameter  $\beta \in \mathbb{R}$  characterizes the strength of the interaction. When  $U$  is bounded, the homogeneous Dirichlet boundary conditions (i.e.,  $\phi|_{\partial U} = 0$ ) can be imposed. In the following, we assume that all wave functions involved below are real-valued functions for simplicity.

The stationary state of a BEC is usually defined as the eigenfunction  $\phi$  to the Euler–Lagrange equation (or time-independent GPE) [3]

$$-\frac{1}{2}\Delta\phi + V(\mathbf{x})\phi + \beta|\phi|^2\phi = \mu\phi, \quad (5.2)$$

under the normalization constraint

$$\|\phi\|^2 := \int_U |\phi(\mathbf{x})|^2 d\mathbf{x} = 1, \quad (5.3)$$

with  $\mu$  the corresponding eigenvalue or chemical potential. When  $\phi$  is an eigenfunction of (5.2)-(5.3), the corresponding chemical potential is given as

$$\mu(\phi) = \int_U \left( \frac{1}{2}|\nabla\phi|^2 + V(\mathbf{x})|\phi|^2 + \beta|\phi|^4 \right) d\mathbf{x} = E(\phi) + \frac{\beta}{2} \int_U |\phi|^4 d\mathbf{x}. \quad (5.4)$$

The ground state is a stationary state with the lowest value of GP energy functional  $E$ , while stationary states with higher energies are called excited states [3]. Noticing that  $E'(\phi) = -\Delta\phi + 2V(\mathbf{x})\phi + 2\beta|\phi|^2\phi$  and setting  $G(\phi) = \|\phi\|^2 - 1$ , we have  $G'(\phi) = 2\phi$ , and (5.2)-(5.3) turns to be

$$E'(\phi) = \mu G'(\phi), \quad G(\phi) = 0. \quad (5.5)$$

Thus, all eigenfunctions of (5.2)-(5.3) are exactly the constrained critical points of the GP energy functional  $E$  (5.1) on the unit spherical manifold  $S = \{\phi \in L^2(U) : \phi|_{\partial U} = 0, G(\phi) = \|\phi\|^2 - 1 = 0, E(\phi) < \infty\}$ . The ground state is the constrained minimizer of  $E$  (5.1) on  $S$ . Since constrained saddle points possess higher energy than that of the ground state, they are sure to be excited states. Although there may be excited states that are not constrained saddle points, such as constrained local minima with higher energies than that of the ground state, here we only consider the excited states corresponding to constrained saddle points of the GP energy functional  $E$ .

Taking  $\langle \cdot, \cdot \rangle$  as the real  $L^2$  inner product (or duality pairing), the tangent space of the constraint manifold  $S$  at  $\phi \in S$  is  $T_\phi S = \{v \in L^2(U) : \langle G'(\phi), v \rangle = 0\} = \text{span}\{\phi\}^\perp$ . For  $\phi \in S$ , the orthogonal projection operator from  $L^2(U)$  onto  $T_\phi S$  is  $P_\phi = I - (\phi \otimes \phi)$ . Then, the projected gradient of the energy functional  $E$  at  $\phi$  reads as

$$F(\phi) := P_\phi E'(\phi) = E'(\phi) - \mu(\phi)G'(\phi) = -\Delta\phi + 2V(\mathbf{x})\phi + 2\beta|\phi|^2\phi - 2\mu(\phi)\phi, \quad (5.6)$$

with  $\mu(\phi) = \frac{1}{2}\langle E'(\phi), \phi \rangle$  given in (5.4). The effective and projected Hessian operators at  $\phi \in S$  are, respectively, given as  $H(\phi) = E''(\phi) - \mu(\phi)G''(\phi)$  and  $\hat{H}(\phi) = P_\phi H(\phi)P_\phi$  where  $E''(\phi) = -\Delta + 2(V(\mathbf{x}) + 3\beta|\phi|^2)I$  and  $G''(\phi) = 2I$  with  $I$  the identity operator.

We remark that any constrained saddle point must be an excited state, thus we call an index- $k$  constrained saddle point  $\phi_k$  an *index- $k$  excited state*. Now one can distinguish the ground state  $\phi_g \in S$  and different excited states according to their energies, chemical potentials (i.e., eigenvalues), and Morse indices. A very interesting question is whether the index- $k$  excited state  $\phi_k$  is precisely the  $k$ -th *excited state* in the sense that

$$E(\phi_g) < E(\phi_1) < E(\phi_2) < \cdots < E(\phi_k) < \cdots, \quad (5.7)$$

and/or whether it is the  $k$ -th *eigenstate* such that

$$\mu(\phi_g) < \mu(\phi_1) < \mu(\phi_2) < \cdots < \mu(\phi_k) < \cdots. \quad (5.8)$$

### 5.1. Properties of excited states in linear case

For the linear case (i.e.,  $\beta = 0$ ), the nonlinear eigenvalue problem (5.2)-(5.3) reduces to

$$-\frac{1}{2}\Delta\phi + V(\mathbf{x})\phi = \mu\phi, \quad G(\phi) = \|\phi\|^2 - 1 = 0, \quad \mathbf{x} \in U \quad (5.9)$$

with homogeneous Dirichlet boundary conditions  $\phi|_{\partial U} = 0$ , and the energy (5.1) and the chemical potential (5.4) are identical. As a result, (5.7) and (5.8) are completely equivalent.

The following result provides an exact characterization for all excited states in linear case.

**Theorem 5.1.** *Assume that  $U$  is a bounded domain with Lipschitz boundary,  $0 \leq V(\mathbf{x}) \in L^\infty(U)$ ,  $\beta = 0$ , and  $\phi_* \in S$  is an eigenfunction of the linear eigenproblem (5.9) with  $\mu_* = \mu(\phi_*) = E(\phi_*)$  the corresponding eigenvalue. Let  $0 < \mu_0 < \mu_1 \leq \mu_2 \leq \dots$  be all the eigenvalues with  $\phi_0, \phi_1, \phi_2, \dots$  the corresponding orthonormal eigenfunctions of the linear eigenproblem (5.9). Then  $\phi_*$  is an index- $k$  ( $k = 1, 2, \dots$ ) excited state if and only if  $\mu_{k-1} < \mu_* = \mu_k$ . Moreover, the unstable tangent subspace of an index- $k$  excited state  $\phi_*$  is  $T^-(\phi_*) = \text{span}\{\phi_0, \phi_1, \dots, \phi_{k-1}\}$ .*

*Proof.* Denote  $A := -\frac{1}{2}\Delta + V(\mathbf{x})I$ . According to the spectral theory of uniformly elliptic operators [23], the set of all eigenfunctions of  $A$  forms a complete basis of  $L^2(U)$ . Since  $A\phi_* = \mu_*\phi_*$ , we have  $H(\phi_*) = -\Delta + 2(V(\mathbf{x}) - \mu_*)I = 2(A - \mu_*I)$ , and therefore,  $H(\phi_*)\phi_* = 2(A\phi_* - \mu_*\phi_*) = 0$ . Then, for any  $\xi \in T_{\phi_*}S$ , noting that  $P_{\phi_*}\xi = \xi$ , we have

$$\begin{aligned} \hat{H}(\phi_*)\xi &= P_{\phi_*}H(\phi_*)\xi = H(\phi_*)\xi - \langle \phi_*, H(\phi_*)\xi \rangle \phi_* \\ &= H(\phi_*)\xi - \langle H(\phi_*)\phi_*, \xi \rangle \phi_* = H(\phi_*)\xi = 2(A - \mu_*I)\xi, \end{aligned}$$

Thus,  $\hat{H}(\phi_*) = 2(A - \mu_*I) : T_{\phi_*}S \rightarrow T_{\phi_*}S$ .

*Necessity.* Suppose that  $\phi_*$  is an index- $k$  excited state. Then the linear operator  $\hat{H}(\phi_*)$  has exactly  $k$  negative eigenvalues. Let  $\lambda_0 \leq \lambda_1 \leq \dots \leq \lambda_{k-1} < 0 \leq \lambda_k \leq \lambda_{k+1} \leq \dots$  be all eigenvalues of  $\hat{H}(\phi_*)$  with  $\{\eta_j\}_{j=0}^\infty \subset T_{\phi_*}S$  the corresponding orthonormal eigenfunctions. Then  $L^2(U) = \text{span}\{\phi_*\} \oplus T_{\phi_*}S = \text{span}\{\phi_*, \eta_j, j = 0, 1, \dots\}$ . Noting that  $A\phi_* = \mu_*\phi_*$  and

$$A\eta_j = \left( \mu_*I + \frac{1}{2}\hat{H}(\phi_*) \right) \eta_j = \left( \mu_* + \frac{\lambda_j}{2} \right) \eta_j, \quad j = 0, 1, \dots,$$

one obtains that all eigenvalues of  $A$  are

$$\mu_* + \frac{\lambda_0}{2} \leq \mu_* + \frac{\lambda_1}{2} \leq \dots \leq \mu_* + \frac{\lambda_{k-1}}{2} < \mu_* \leq \mu_* + \frac{\lambda_k}{2} \leq \mu_* + \frac{\lambda_{k+1}}{2} \leq \dots$$

Therefore,  $\mu_{k-1} = \mu_* + \frac{\lambda_{k-1}}{2} < \mu_* = \mu_k$ .

*Sufficiency.* Suppose that  $\mu_{k-1} < \mu_* = \mu_k$ . Without loss of generality, assume  $\phi_* = \phi_k$ . Then  $T_{\phi_*}S = \text{span}\{\phi_*\}^\perp = \text{span}\{\phi_0, \phi_1, \dots, \phi_{k-1}, \phi_{k+1}, \dots\}$ . Note that

$$\hat{H}(\phi_*)\phi_i = 2(A - \mu_kI)\phi_i = 2(\mu_i - \mu_k)\phi_i, \quad i = 0, 1, \dots, k-1, \dots, k+1, \dots$$

The maximum negative definite subspace of the linear operator  $\hat{H}(\phi_*) : T_{\phi_*}S \rightarrow T_{\phi_*}S$  is given as  $T^- = \text{span}\{\phi_0, \phi_1, \dots, \phi_{k-1}\}$ . Thus, the Morse index of  $\phi_*$  is  $\dim(T^-) = k$ , i.e.,  $\phi_*$  is an index- $k$  excited state.  $\square$

**Remark 5.2.** *The result of Theorem 5.1 can be extended to the cases when  $U = \mathbb{R}^d$  and the potential  $V(\mathbf{x})$  satisfies:  $V(\mathbf{x})$  is continuous in  $\mathbb{R}^d$ ,  $V(\mathbf{x}) \geq 0$  and  $\lim_{|\mathbf{x}| \rightarrow \infty} V(\mathbf{x}) = \infty$ . In addition, Theorem 5.1 can also be proved by applying the generalized Courant-Fischer formula or min-max principle for self-adjoint operators (see, e.g., [32]).*

Noting that, when  $\beta = 0$ ,  $E(\phi) = \mu(\phi)$ , we have the following corollaries.

**Corollary 5.3.** *Under assumptions of Theorem 5.1, if further  $\mu_0 < \mu_1 < \dots < \mu_k$ , i.e.,  $\mu_0, \mu_1, \dots, \mu_{k-1}$  are single-fold eigenvalues, then  $\phi_*$  is an index- $k$  excited state if and only if it is the  $k$ -th eigenstate defined in (5.8) (equivalently, it is the  $k$ -th excited state defined in (5.7)). In particular, since  $\mu_0$  is single-fold, the index-1 excited state is exactly the first excited state and the first eigenstate.*

**Corollary 5.4.** *Under assumptions of Theorem 5.1, all excited states are constrained saddle points, and the ground state  $\phi_g$  (up to the sign) is the only possible constrained local minimizer and thus the constrained global minimizer.*

**Example 5.5.** *Assume  $\beta = 0$ . Take  $V(\mathbf{x})$  as the box potential:*

$$V_{\text{box},L}(\mathbf{x}) = \begin{cases} 0, & \mathbf{x} \in U := [0, L]^d, \\ \infty, & \mathbf{x} \notin U, \end{cases} \quad \mathbf{x} = (x_1, x_2, \dots, x_d)^T$$

with  $L > 0$  the width of the box. The eigenpairs of the linear eigenproblem (5.9) are

$$\phi_{\mathbf{j}}^{\text{box}}(\mathbf{x}) = \left(\frac{2}{L}\right)^{d/2} \prod_{\alpha=1}^d \sin \frac{(j_\alpha + 1)\pi x_\alpha}{L}, \quad \mathbf{x} \in U, \quad \mu_{\mathbf{j}}^{\text{box}} = \frac{\pi^2}{2L^2} \sum_{\alpha=1}^d (j_\alpha + 1)^2, \quad (5.10)$$

for all  $\mathbf{j} = (j_1, j_2, \dots, j_d) \in \mathbb{N}^d$ . From Theorem 5.1 and Corollary 5.3, we have the following conclusions:

- (i)  $\phi_{\mathbf{0}}^{\text{box}}$  is the ground state.
- (ii) When  $d = 1$ , we have  $\mu_j^{\text{box}} = \frac{\pi^2}{2L^2}(j+1)^2$ ,  $j = 0, 1, \dots$  and therefore  $\mu_0^{\text{box}} < \mu_1^{\text{box}} < \mu_2^{\text{box}} < \mu_3^{\text{box}} < \dots$ . Thus  $\phi_k^{\text{box}}$  ( $k \geq 1$ ) is exactly an index- $k$  excited state as well as the  $k$ -th excited state (and the  $k$ -th eigenstate) with its unstable tangent subspace  $T^-(\phi_k^{\text{box}}) = \text{span}\{\phi_j^{\text{box}} : j = 0, 1, \dots, k-1\}$ .
- (iii) When  $d = 2$ , the first few stationary states with corresponding energy levels and Morse indices are listed in Table 1. Thus any  $\phi \in S \cap \text{span}\{\phi_{(1,0)}^{\text{box}}, \phi_{(0,1)}^{\text{box}}\}$  is an index-1 excited state as well as the first excited state with its unstable tangent subspace spanned by  $\phi_{(0,0)}^{\text{box}}$ . However, the second excited state  $\phi_{(1,1)}^{\text{box}}$  is actually an index-3 excited state with its unstable tangent subspace spanned by  $\phi_{(0,0)}^{\text{box}}$ ,  $\phi_{(1,0)}^{\text{box}}$  and  $\phi_{(0,1)}^{\text{box}}$ . In general, as shown in Table 1, the order of energies or chemical potentials of excited states is accordance with that of Morse indices.

Table 1: Energy levels and indices of the first few excited states for the box potential in 2D with  $\beta = 0$ .

$\mathbf{j}$	(0, 0)	(1, 0), (0, 1)	(1, 1)	(2, 0), (0, 2)	(2, 1), (1, 2)	(3, 0), (0, 3)	(2, 2)
$(2L^2/\pi^2)\mu_{\mathbf{j}}^{\text{box}}$	2	5	8	10	13	17	18
energy levels	0	1	2	3	4	5	6
indices	0	1	3	4	6	8	10

**Example 5.6.** *Assume  $\beta = 0$ . Take  $V(\mathbf{x})$  as the harmonic oscillator potential:*

$$V_{\text{ho}}(\mathbf{x}) = \frac{1}{2}|\mathbf{x}|^2 = \frac{1}{2} \sum_{\alpha=1}^d x_\alpha^2, \quad \mathbf{x} = (x_1, x_2, \dots, x_d)^T \in U = \mathbb{R}^d.$$

Then the eigenpairs of the linear eigenproblem (5.9) are given as

$$\phi_{\mathbf{j}}^{\text{ho}}(\mathbf{x}) = \prod_{\alpha=1}^d \hat{h}_{j_\alpha}(x_\alpha), \quad \mu_{\mathbf{j}}^{\text{ho}} = |\mathbf{j}| + \frac{d}{2}, \quad \mathbf{j} = (j_1, j_2, \dots, j_d) \in \mathbb{N}^d, \quad (5.11)$$

where  $|\mathbf{j}| := \sum_{\alpha=1}^d j_\alpha$ ,  $\hat{h}_j(x)$  are the Hermite functions:

$$\hat{h}_j(x) = \frac{1}{\pi^{1/4} \sqrt{2^j j!}} e^{-x^2/2} h_j(x), \quad j = 0, 1, 2, \dots, \quad (5.12)$$

with  $h_j(x) = (-1)^j e^{x^2} \frac{d^j}{dx^j} (e^{-x^2})$  the Hermite polynomials. Obviously,  $\phi_{\mathbf{0}}^{\text{ho}}$  is the ground state. From Theorem 5.1 and Corollary 5.3, any function  $\phi \in S \cap \text{span}\{\phi_{\mathbf{j}}^{\text{ho}} : \mathbf{j} \in \mathbb{N}^d, |\mathbf{j}| = k\}$  is the  $k$ -th excited state and an index- $i_d(k)$  excited state with its unstable tangent subspace  $T^-(\phi) = \text{span}\{\phi_{\mathbf{j}}^{\text{ho}} : \mathbf{j} \in \mathbb{N}^d, |\mathbf{j}| \leq k-1\}$ , where

$$i_d(k) = \#\{\mathbf{j} \in \mathbb{N}^d : |\mathbf{j}| \leq k-1\} = \begin{cases} k, & d = 1, \\ \frac{1}{2}k(k+1), & d = 2, \\ \frac{1}{6}k(k+1)(k+2), & d = 3. \end{cases}$$

It is observed that,  $i_d(k) = k$  if either  $d = 1$  or  $k = 0, 1$ ; Otherwise,  $i_d(k) > k$ .

### 5.2. CGAD for single-component BECs and its time discretization

We now propose the formulation of the CGAD for computing excited states of a single-component BEC and its efficient time discretization scheme.

Let  $\phi \in S$  be an approximation of an index- $k$  excited state and  $\{v_i\}_{i=1}^k \subset T_\phi S$  be the approximations of corresponding unstable tangent directions. Noting that  $G'(\phi) = 2\phi$  and  $G''(\phi) = 2I$ , by applying the CGAD (3.11) to the single-component BEC model, we obtain

$$\begin{cases} \gamma_0 \partial_t \phi(\mathbf{x}, t) = -F(\phi) + 2 \sum_{j=1}^k \langle F(\phi), v_j \rangle v_j, \\ \gamma_i \partial_t v_i(\mathbf{x}, t) = -\hat{H}(\phi) v_i + \sum_{j=1}^i \lambda_{ij} v_j + 2\bar{\lambda}_i \phi, \quad i = 1, 2, \dots, k, \end{cases} \quad (5.13)$$

where  $\gamma_i > 0$  ( $i = 0, 1, \dots, k$ ) are relaxation parameters, Lagrange multipliers  $\lambda_{ij}$  and  $\bar{\lambda}_i$  are given as

$$\lambda_{ij} = \left(1 + \frac{\gamma_i}{\gamma_j} - \delta_{ij}\right) \langle \hat{H}(\phi) v_i, v_j \rangle, \quad \bar{\lambda}_i = \frac{\gamma_i}{2\gamma_0 \|\phi\|^2} \left\langle v_i, F(\phi) - 2 \sum_{j=1}^k \langle F(\phi), v_j \rangle v_j \right\rangle, \quad 1 \leq j \leq i \leq k.$$

Lemma 3.2 states that (5.13) preserves constraints  $\phi \in S$ ,  $v_i \in T_\phi S$ ,  $\langle v_i, v_j \rangle = \delta_{ij}$ , i.e.,

$$\|\phi\|^2 = 1, \quad \langle \phi, v_i \rangle = 0, \quad \langle v_i, v_j \rangle = \delta_{ij}, \quad 1 \leq j \leq i \leq k. \quad (5.14)$$

Using (5.14), we have  $\langle F(\phi), v_i \rangle = \langle E'(\phi), P_\phi v_i \rangle = \langle E'(\phi), v_i \rangle$ ,

$$\begin{aligned} \hat{H}(\phi) v_i &= P_\phi (E''(\phi) - 2\mu(\phi)I) P_\phi v_i = E''(\phi) v_i - \langle E''(\phi) \phi, v_i \rangle \phi - 2\mu(\phi) v_i, \\ \lambda_{ij} &= \left(1 + \frac{\gamma_i}{\gamma_j} - \delta_{ij}\right) \langle E''(\phi) v_i, v_j \rangle - 2\mu(\phi) \delta_{ij}, \quad \bar{\lambda}_i = -\frac{\gamma_i}{2\gamma_0} \langle E'(\phi), v_i \rangle. \end{aligned}$$

Noting that  $E'(\phi) = -\Delta\phi + 2V(\mathbf{x})\phi + 2\beta|\phi|^2\phi$ ,  $E''(\phi) = -\Delta + 2(V(\mathbf{x}) + 3\beta|\phi|^2)I$ , by taking  $\gamma_0 = \gamma_1 = \dots = \gamma_k = 2$ , (5.13) can be simplified as

$$\begin{cases} \partial_t \phi(\mathbf{x}, t) = \frac{1}{2} \Delta \phi - V(\mathbf{x})\phi - \beta|\phi|^2\phi + \mu(\phi)\phi + 2 \sum_{j=1}^k \xi_j v_j, \\ \partial_t v_i(\mathbf{x}, t) = \frac{1}{2} \Delta v_i - V(\mathbf{x})v_i - 3\beta|\phi|^2 v_i + \sigma_i \phi + \sum_{j=1}^i \nu_{ij} v_j, \quad i = 1, 2, \dots, k, \end{cases} \quad (5.15)$$

where

$$\xi_i = \xi_i(\phi, v_i) = \int_U \left( \frac{1}{2} \nabla \phi \cdot \nabla v_i + V(\mathbf{x}) \phi v_i + \beta |\phi|^2 \phi v_i \right) d\mathbf{x}, \quad (5.16)$$

$$\nu_{ij} = \nu_{ij}(\phi, v_i, v_j) = (2 - \delta_{ij}) \int_U \left( \frac{1}{2} \nabla v_i \cdot \nabla v_j + V(\mathbf{x}) v_i v_j + 3\beta |\phi|^2 v_i v_j \right) d\mathbf{x}, \quad (5.17)$$

$$\sigma_i = \sigma_i(\phi, v_i) = 2\beta \int_U |\phi|^2 \phi v_i d\mathbf{x}, \quad 1 \leq j \leq i \leq k. \quad (5.18)$$

Various suitable numerical schemes could be used to solve (5.15). For simplicity and efficiency, we use the prediction-correction strategy to discretize (5.15) in time with a (semi-implicit) backward-forward Euler scheme followed by the Gram–Schmidt orthonormalization process to preserve the constraints (5.14) in the discretized level.

The initial data  $(\phi^0, v_1^0, \dots, v_k^0)$  is chosen satisfying the constraints (5.14). Set  $t_n = n\tau$ ,  $n = 0, 1, \dots$ , with  $\tau > 0$  a selected time step length. Let  $(\phi^n, v_1^n, \dots, v_k^n)$  be the numerical approximation of the solution of (5.15) at  $t = t_n$ . We adopt the following iterative scheme to compute  $(\phi^{n+1}, v_1^{n+1}, \dots, v_k^{n+1})$  from  $(\phi^n, v_1^n, \dots, v_k^n)$ :

$$\begin{cases} \frac{\tilde{\phi}^{n+1} - \phi^n}{\tau} = \frac{1}{2} \Delta \tilde{\phi}^{n+1} - V(\mathbf{x}) \phi^n - \beta |\phi^n|^2 \phi^n + \mu^n \phi^n + 2 \sum_{j=1}^k \xi_j^n v_j^n, \\ \frac{\tilde{v}_i^{n+1} - v_i^n}{\tau} = \frac{1}{2} \Delta \tilde{v}_i^{n+1} - V(\mathbf{x}) v_i^n - 3\beta |\phi^n|^2 v_i^n + \sigma_i^n \phi^n + \sum_{j=1}^i \nu_{ij}^n v_j^n, \quad i = 1, 2, \dots, k, \\ [\phi^{n+1}, v_1^{n+1}, \dots, v_k^{n+1}] = \text{GSON} \left( [\tilde{\phi}^{n+1}, \tilde{v}_1^{n+1}, \dots, \tilde{v}_k^{n+1}] \right), \end{cases} \quad (5.19)$$

where  $\mu^n = \mu(\phi^n)$  (5.4),  $\xi_i^n = \xi_i(\phi^n, v_i^n)$  (5.16),  $\nu_{ij}^n = \nu_{ij}(\phi^n, v_i^n, v_j^n)$  (5.17),  $\sigma_i^n = \sigma_i(\phi^n, v_i^n)$  (5.18), and GSON denotes the standard Gram–Schmidt orthonormalization procedure to preserve that  $(\phi^{n+1}, v_1^{n+1}, \dots, v_k^{n+1})$  satisfies the constraints (5.14). We remark that GSON in (5.19) can also be implemented with its variants (e.g., the modified Gram-Schmidt algorithm or the Gram-Schmidt with re-orthogonalization) to overcome the numerical instability (of round-off errors) that may occur in some extreme and ill-conditioned cases. We choose the current version of GSON (i.e., the standard Gram–Schmidt procedure) in our numerical experiments for simplicity since it works well for all cases of this paper.

Clearly, the main computational cost of the scheme (5.19) at each time step is to solve a completely decoupled system of  $k + 1$  linear elliptic equations with constant coefficients. All equations in the system take the same form:  $-\frac{\tau}{2} \Delta u + u = f$ , only with different right-hand-side terms  $f$ . Thus, they can be solved very efficiently, especially when a fast Poisson solver (e.g., fast Fourier transform) and parallel algorithms are available.

In our numerical computation, the iterative scheme (5.19) for computing index- $k$  excited states of a single-component BEC is stopped when the following stopping criteria are satisfied:

$$\|F^n\|_\infty < \varepsilon, \quad \frac{\|\phi^{n+1} - \phi^n\|_\infty}{\tau} < \varepsilon, \quad \frac{\|v_i^{n+1} - v_i^n\|_\infty}{\tau} < \varepsilon, \quad i = 1, 2, \dots, k, \quad (5.20)$$

where  $F^n := -\frac{1}{2} \Delta \phi^n + V(\mathbf{x}) \phi^n + \beta |\phi^n|^2 \phi^n - \mu^n \phi^n$  is the residual of the Euler–Lagrange equation (5.2) at  $(\mu^n, \phi^n)$ , and  $\varepsilon > 0$  is a given tolerance.

**Remark 5.7.** *In order to improve the computational efficiency of the scheme (5.19), one can introduce a suitable stabilization term [5, 4, 3] with constant coefficient for each equation in (5.19) so that the larger step length can be chosen in practice. Our numerical experiments show that such a stabilized version of (5.19) is efficient. However, due to the limit of page, we leave the rigorous*



stability analysis for the scheme (5.19) to future work. It is worthwhile to mention that, on the stability at large step size for index-1 saddle points of functionals, one existing approach is to use the iterative minimization formulation (IMF) [22] to have a sequence of minimization problems and to design a convex splitting method [25] to minimize the auxiliary functional at each cycle of the IMF.

**Remark 5.8.** If one takes  $k = 0$  (i.e., remove all approximations of the unstable directions  $v_i$ ) in (5.15), then the CGAD (5.15) reduces to the continuous normalized gradient flow (CNGF) [5] for computing the ground state of single-component BECs, and the corresponding time discretization scheme (5.19) becomes the backward-forward Euler scheme (followed by a normalization step) for the CNGF (see [33]).

### 5.3. Numerical results

We now report the numerical results of the excited states of single-component BECs in 1D and 2D computed by the numerical scheme (5.19) of the CGAD. In particular, the asymptotic properties of the energies and chemical potentials of excited states corresponding to different parameters  $\beta$  are investigated. Meanwhile, the energies and chemical potentials of the ground state and excited states with different Morse indices are compared.

In our experiments, the following three types of potentials are considered [3]:

(i) the box potential

$$V_{\text{box}}(\mathbf{x}) = \begin{cases} 0, & \mathbf{x} \in U = [0, 1]^d, \\ \infty, & \mathbf{x} \notin U, \end{cases} \quad d = 1, 2, \quad (5.21)$$

(ii) the harmonic oscillator potential

$$V_{\text{ho}}(\mathbf{x}) = \begin{cases} x^2/2, & d = 1, \\ (x^2 + y^2)/2, & d = 2, \end{cases} \quad (5.22)$$

(iii) the harmonic oscillator plus optical lattice potential

$$V_{\text{hol}}(\mathbf{x}) = V_{\text{ho}}(\mathbf{x}) + \begin{cases} \kappa \sin^2(\pi x/4), & d = 1, \\ \kappa (\sin^2(\pi x/4) + \sin^2(\pi y/4)), & d = 2, \end{cases} \quad (5.23)$$

with  $\kappa > 0$  the depth of the optical lattice.

We compute excited states by the numerical scheme (5.19) of CGAD with time step  $\tau = 0.01$ . The stopping criterion (5.20) with  $\varepsilon = 10^{-12}$  is applied. For numerical comparison, we also use the normalized gradient flow [5, 33] to compute the ground state. All algorithms are implemented on a bounded domain  $U \subset \mathbb{R}^d$  ( $d = 1, 2$ ) with the spatial sine-pseudospectral discretization (see, e.g., [4]) with mesh size  $h = \frac{1}{32}$ .

#### 5.3.1. Numerical results in 1D

**Example 5.9.** In this example, the first few excited states with the box potential  $V(x) = V_{\text{box}}(x)$  (5.21) in 1D and various interaction coefficient  $\beta$  are computed. Then, the asymptotic properties of their energies and chemical potentials are studied.

Let  $\phi_k^\beta$  be the numerical index- $k$  excited state for specified  $\beta$  computed with the initial data:  $\phi^0(x) = \phi_k^{\text{box}}(x) = \sqrt{2} \sin((k+1)\pi x)$  and  $v_i^0(x) = \phi_{i-1}^{\text{box}}(x) = \sqrt{2} \sin(i\pi x)$ ,  $x \in [0, 1]$ ,  $i = 1, 2, \dots, k$ . Fig. 3 plots the profiles of  $\phi_k^\beta(x)$ ,  $k = 1, 2, \dots, 9$ , with different  $\beta = 100, 3200, 102400$ . The energies and chemical potentials of  $\phi_g^\beta$  and  $\phi_k^\beta$  ( $k = 1, 2, \dots, 9$ ) for various  $\beta$  are listed in Table 2 (the initial

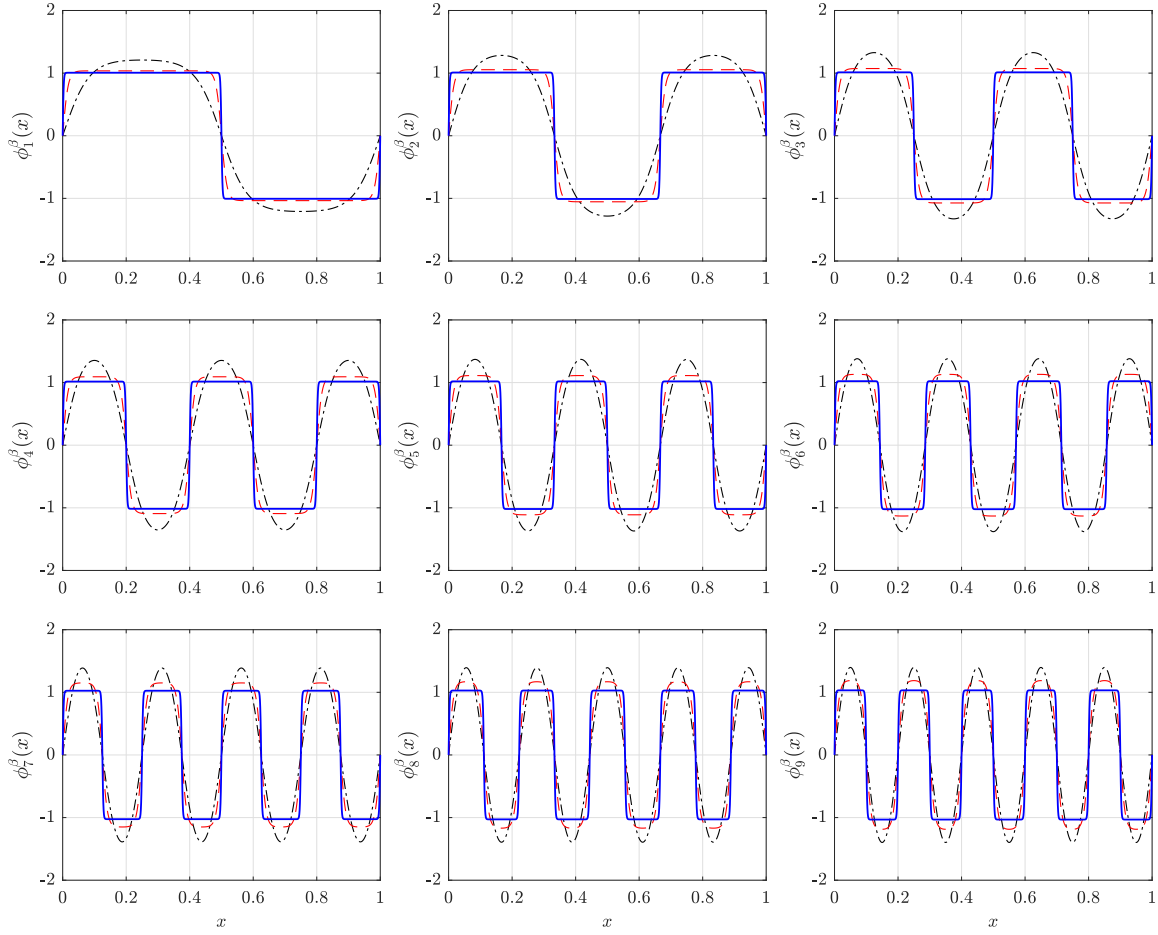


Figure 3: Profiles of index- $k$  ( $k = 1, 2, \dots, 9$ ) excited states  $\phi_k^\beta(x)$  in Example 5.9 with  $\beta = 100$  (black dash-dot lines), 3200 (red dash lines) and 102400 (blue solid lines).

Table 2: Energies and chemical potentials of the ground state  $\phi_g^\beta$  and excited states  $\phi_k^\beta$  ( $k = 1, 2, \dots, 9$ ) versus the interaction coefficient  $\beta$  in Example 5.9.

$\beta$	$E(\phi_g^\beta)$	$E(\phi_1^\beta)$	$E(\phi_2^\beta)$	$E(\phi_3^\beta)$	$E(\phi_4^\beta)$	$E(\phi_5^\beta)$	$E(\phi_6^\beta)$	$E(\phi_7^\beta)$	$E(\phi_8^\beta)$	$E(\phi_9^\beta)$
0	4.93480	19.7392	44.4132	78.9568	123.370	177.653	241.805	315.827	399.719	493.480
0.01	4.94230	19.7467	44.4207	78.9643	123.378	177.660	241.813	315.835	399.726	493.488
1	5.67870	20.4876	45.1625	79.7064	124.120	178.403	242.555	316.577	400.469	494.230
100	65.5472	86.4930	114.450	150.756	196.171	251.062	315.606	389.893	473.972	567.870
1600	855.384	915.080	979.419	1048.75	1123.46	1203.94	1290.61	1383.89	1484.21	1591.96
12800	6552.87	6709.84	6871.03	7036.56	7206.52	7381.05	7560.27	7744.28	7933.24	8127.25
102400	51628.7	52061.4	52498.2	52939.1	53384.1	53833.4	54286.8	54744.6	55206.6	55673.0
$\beta$	$\mu(\phi_g^\beta)$	$\mu(\phi_1^\beta)$	$\mu(\phi_2^\beta)$	$\mu(\phi_3^\beta)$	$\mu(\phi_4^\beta)$	$\mu(\phi_5^\beta)$	$\mu(\phi_6^\beta)$	$\mu(\phi_7^\beta)$	$\mu(\phi_8^\beta)$	$\mu(\phi_9^\beta)$
0	4.93480	19.7392	44.4132	78.9568	123.370	177.653	241.805	315.827	399.719	493.480
0.01	4.94980	19.7542	44.4282	78.9718	123.385	177.668	241.820	315.842	399.734	493.495
1	6.41672	21.2345	45.9111	80.4557	124.869	179.152	243.305	317.327	401.219	494.980
100	122.100	148.803	180.961	219.961	267.060	323.031	388.293	463.078	547.512	641.672
1600	1682.02	1768.20	1858.67	1953.60	2053.11	2157.38	2266.55	2380.85	2500.53	2625.93
12800	13028.3	13260.6	13497.1	13737.7	13982.5	14231.6	14484.9	14742.7	15004.9	15271.6
102400	103042	103688	104338	104992	105650	106313	106979	107650	108324	109003

guess for the ground state  $\phi_g^\beta$  is taken as  $\phi^0(x) = \phi_0^{\text{box}}(x) = \sqrt{2}\sin(\pi x)$ . Moreover, the asymptotic behaviors of the energies of excited states in the weakly repulsive interaction regime, i.e.,  $0 < \beta \ll 1$ , and the strongly repulsive interaction regime, i.e.,  $\beta \gg 1$ , are shown in Fig. 4.

From the experimental results that are partially shown in Figs. 3-4 and Table 2, we have the

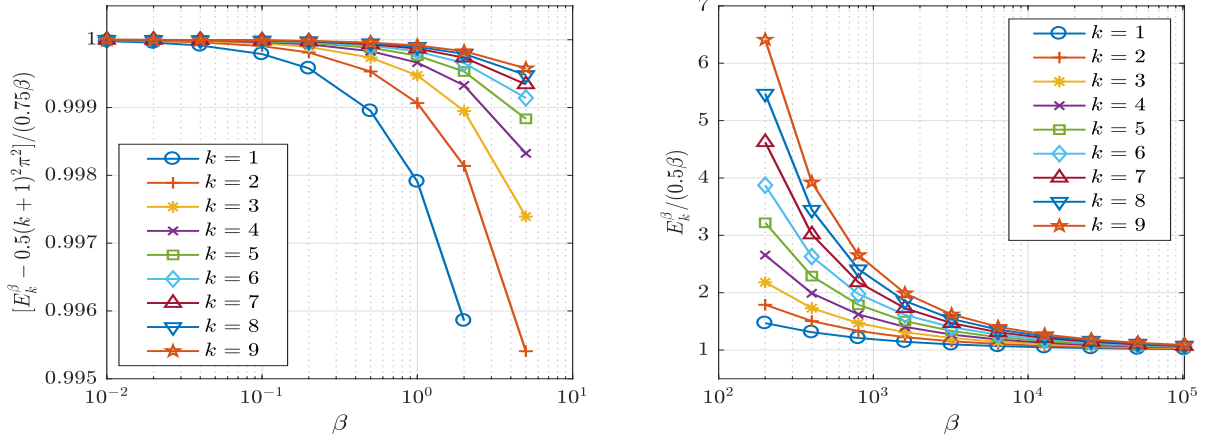


Figure 4: Asymptotic behaviors of the energies for index- $k$  ( $k = 1, 2, \dots, 9$ ) excited states for the weakly (left) and strongly (right) repulsive interaction regime in Example 5.9.

following numerical observations:

- (i) Fig. 3 shows that the index- $k$  excited state  $\phi_k^\beta$  is oddly symmetric for  $k = 1, 3, 5, 7, 9$  (i.e.,  $k$  is odd) and evenly symmetric for  $k = 2, 4, 6, 8$  (i.e.,  $k$  is even) with respect to the line  $x = 1/2$ . For relatively small  $\beta$ , the profile of  $\phi_k^\beta(x)$  is similar to that of  $\phi_k^0(x) = \phi_k^{\text{box}}(x) = \sqrt{2} \sin((k+1)\pi x)$ . When  $\beta$  is large,  $\phi_k^\beta(x)$  has precisely two boundary layers and  $k$  interior layers distributed equidistantly. It looks like a piecewise two-valued function that evenly takes  $+1$  and  $-1$ .
- (ii) Table 2 shows that, for any  $\beta \geq 0$ , the excited state with higher Morse index possesses higher energy and larger chemical potential, namely,

$$E(\phi_g^\beta) < E(\phi_1^\beta) < E(\phi_2^\beta) < \dots \iff \mu(\phi_g^\beta) < \mu(\phi_1^\beta) < \mu(\phi_2^\beta) < \dots.$$

Furthermore, for fixed  $k = 1, 2, \dots$ , we observe that

$$\lim_{\beta \rightarrow +\infty} \frac{E(\phi_k^\beta)}{E(\phi_g^\beta)} = 1, \quad \lim_{\beta \rightarrow +\infty} \frac{\mu(\phi_k^\beta)}{\mu(\phi_g^\beta)} = 1 \quad \text{and} \quad \lim_{\beta \rightarrow +\infty} \frac{\mu(\phi_k^\beta)}{E(\phi_k^\beta)} = 2.$$

- (iii) From Fig. 4, one observes that for the weakly repulsive interaction regime,

$$E(\phi_k^\beta) = \frac{(k+1)^2 \pi^2}{2} + \frac{3}{4} \beta + o(\beta) = E(\phi_k^{\text{box}}) + o(\beta),$$

where  $\phi_k^{\text{box}}(x) = \sqrt{2} \sin((k+1)x)$ , while for the strongly repulsive interaction regime,  $E(\phi_k^\beta) \approx \beta/2$ .

These observations are consistent with the results in [6, 7].

**Example 5.10.** We now compute the first few excited states for the harmonic oscillator potential  $V(x) = V_{\text{ho}}(x)$  (5.22) in 1D with various interaction coefficient  $\beta$  and study the asymptotics of their energies and chemical potentials.

The computational domain is taken as  $U = [-16, 16]$ . Let  $\phi_k^\beta$  and  $\phi_g^\beta$  be the numerical index- $k$  excited state and ground state, respectively, for specified  $\beta$ . The initial data for  $\phi_k^\beta$  and  $\phi_g^\beta$  are, respectively, chosen as  $\phi^0(x) = \phi_k^{\text{ho}}(x)$ ,  $v_i^0(x) = \phi_{i-1}^{\text{ho}}(x)$ ,  $i = 1, 2, \dots, k-1$ , and  $\phi^0(x) = \phi_0^{\text{ho}}(x)$ . Fig. 5 plots the profiles of  $\phi_k^\beta(x)$ ,  $k = 1, 2, \dots, 9$ , with different  $\beta = 100, 400, 1600$ . The energies

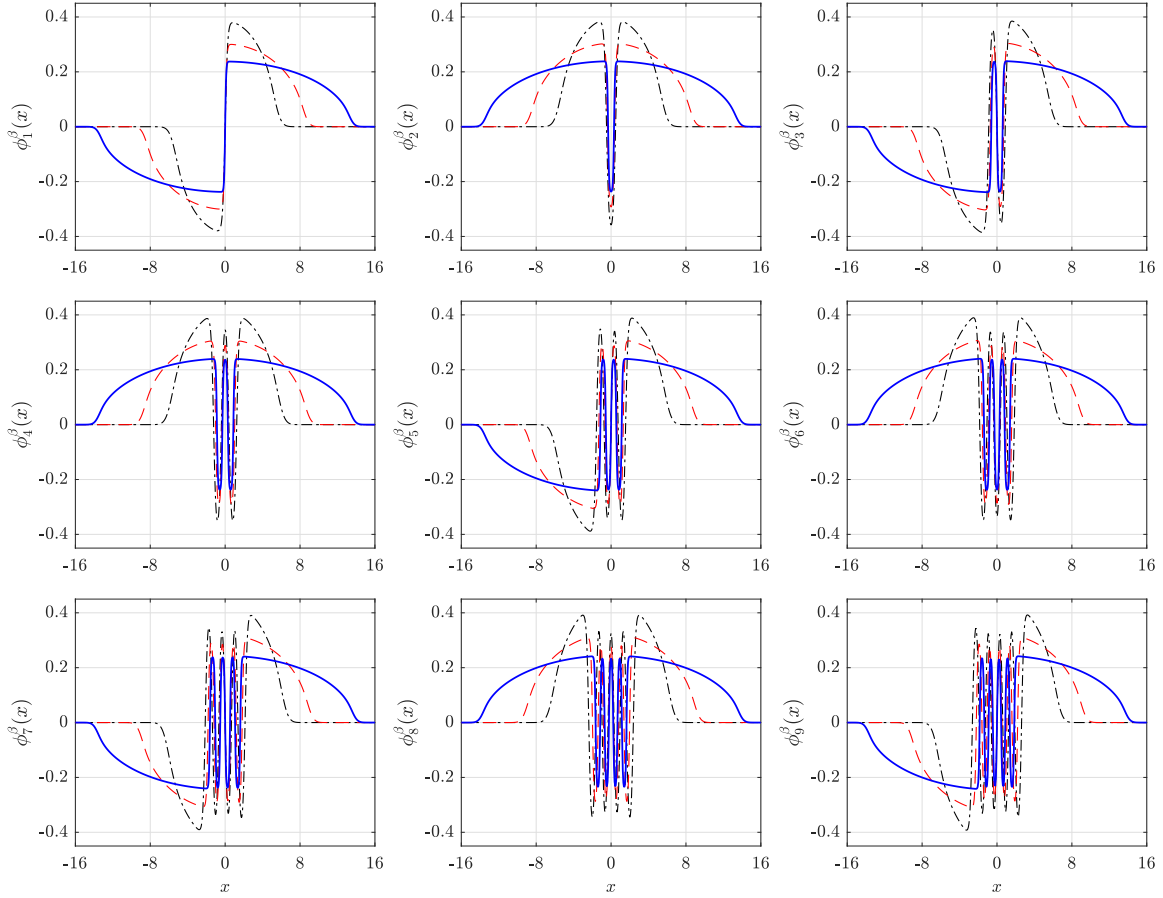


Figure 5: Profiles of index- $k$  ( $k = 1, 2, \dots, 9$ ) excited states  $\phi_k^\beta(x)$  for  $\beta = 100$  (black dash-dot lines), 400 (red dash lines) and 1600 (blue solid lines) in Example 5.10.

Table 3: Energies and chemical potentials of the ground state  $\phi_g^\beta$  and excited states  $\phi_k^\beta$  ( $k = 1, 2, \dots, 9$ ) versus the interaction coefficient  $\beta$  in Example 5.10.

$\beta$	$E(\phi_g^\beta)$	$E(\phi_1^\beta)$	$E(\phi_2^\beta)$	$E(\phi_3^\beta)$	$E(\phi_4^\beta)$	$E(\phi_5^\beta)$	$E(\phi_6^\beta)$	$E(\phi_7^\beta)$	$E(\phi_8^\beta)$	$E(\phi_9^\beta)$
0	0.50000	1.50000	2.50000	3.50000	4.50000	5.50000	6.50000	7.50000	8.50000	9.50000
0.01	0.50199	1.50150	2.50128	3.50115	4.50105	5.50098	6.50093	7.50088	8.50084	9.50081
1	0.68948	1.64655	2.62626	3.61361	4.60467	5.59787	6.59246	7.58800	8.58424	9.58101
10	1.94713	2.76538	3.64568	4.55841	5.49090	6.43654	7.39147	8.35325	9.32029	10.2914
100	8.50853	9.24191	10.0079	10.7989	11.6100	12.4378	13.2797	14.1338	14.9985	15.8725
400	21.3601	22.0777	22.8116	23.5594	24.3196	25.0909	25.8721	26.6626	27.4614	28.2680
1600	53.7855	54.4968	55.2154	55.9407	56.6723	57.4098	58.1528	58.9011	59.6545	60.4127
$\beta$	$\mu(\phi_g^\beta)$	$\mu(\phi_1^\beta)$	$\mu(\phi_2^\beta)$	$\mu(\phi_3^\beta)$	$\mu(\phi_4^\beta)$	$\mu(\phi_5^\beta)$	$\mu(\phi_6^\beta)$	$\mu(\phi_7^\beta)$	$\mu(\phi_8^\beta)$	$\mu(\phi_9^\beta)$
0	0.50000	1.50000	2.50000	3.50000	4.50000	5.50000	6.50000	7.50000	8.50000	9.50000
0.01	0.50398	1.50299	2.50256	3.50229	4.50211	5.50197	6.50186	7.50177	8.50169	9.50162
1	0.86994	1.79015	2.75102	3.72629	4.70870	5.69528	6.68456	7.67572	8.66825	9.66182
10	3.10724	3.86320	4.68057	5.53782	6.42244	7.32672	8.24566	9.17583	10.1148	11.0610
100	14.1343	14.8505	15.5846	16.3352	17.1008	17.8799	18.6713	19.4739	20.2868	21.1092
400	35.5775	36.2881	37.0061	37.7313	38.4636	39.2026	39.9480	40.6998	41.4576	42.2212
1600	89.6319	90.3404	91.0518	91.7662	92.4834	93.2035	93.9265	94.6523	95.3809	96.1123

and chemical potentials of  $\phi_g^\beta$  and  $\phi_k^\beta$  ( $k = 1, 2, \dots, 9$ ) for various  $\beta$  are listed in Table 2. Fig. 6 shows that the asymptotics of the energies of  $\phi_k^\beta$  ( $k = 1, 2, \dots, 9$ ) in both the weakly and strongly repulsive interaction regime.

From the experimental results that are partially shown in Figs. 5-6 and Table 3, we have the following numerical observations:

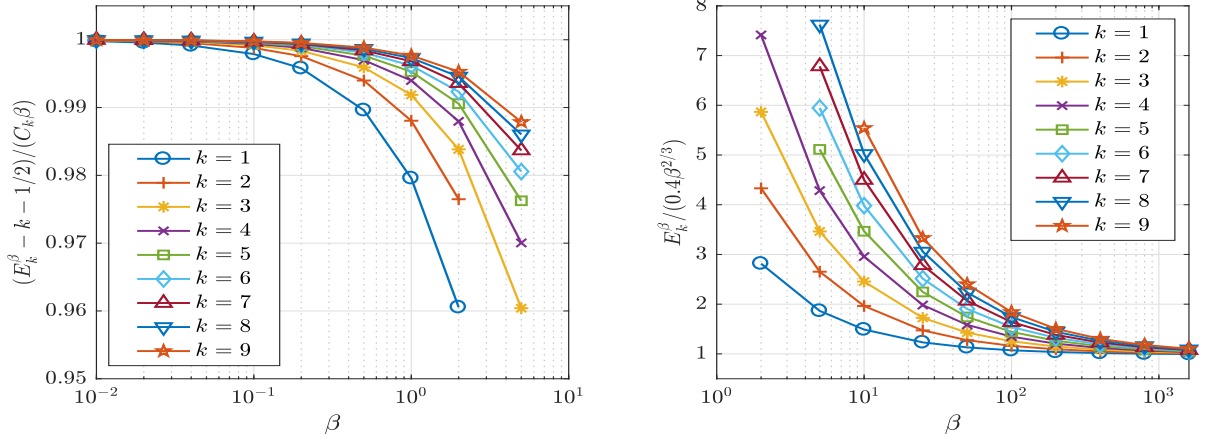


Figure 6: Asymptotic behaviors of the energy for index- $k$  ( $k = 1, 2, \dots, 9$ ) excited states for the weakly (left) and strongly (right) repulsive interaction regime in Example 5.10.

- (i) Fig. 5 shows that the index- $k$  excited state  $\phi_k^\beta$  is precisely an odd function when  $k$  is odd and an even function when  $k$  is even. For relatively small  $\beta$ , the profile of  $\phi_k^\beta(x)$  is similar to that of  $\phi_k^0(x) = \phi_k^{\text{ho}}(x)$ . When  $\beta$  is large,  $\phi_k^\beta(x)$  has exactly  $k$  interior layers or oscillations distributed densely near the center of domain, i.e.,  $x = 0$ , thus the multiscale structures are observed.
- (ii) Table 3 shows that, for any  $\beta \geq 0$ , all of the excited states we obtain have higher energies than that of the ground state. Moreover, the higher Morse indices the excited states have, the higher energy levels they possess. This observation is also available for the relationship between the Morse indices and the chemical potentials of excited states. That is

$$E(\phi_g^\beta) < E(\phi_1^\beta) < E(\phi_2^\beta) < \dots \iff \mu(\phi_g^\beta) < \mu(\phi_1^\beta) < \mu(\phi_2^\beta) < \dots .$$

Meanwhile, for fixed  $k = 1, 2, \dots$ , we observe that

$$\lim_{\beta \rightarrow \infty} \frac{E(\phi_k^\beta)}{E(\phi_g^\beta)} = 1, \quad \lim_{\beta \rightarrow \infty} \frac{\mu(\phi_k^\beta)}{\mu(\phi_g^\beta)} = 1, \quad \lim_{\beta \rightarrow \infty} \frac{\mu(\phi_k^\beta)}{E(\phi_k^\beta)} = \frac{5}{3}.$$

- (iii) Fig. 6 shows that, for the weakly repulsive interaction regime,

$$E(\phi_k^\beta) = k + \frac{1}{2} + C_k \beta + o(\beta) = E(\phi_k^{\text{ho}}) + o(\beta),$$

with  $C_k = \frac{1}{2} \int_{\mathbb{R}} |\phi_k^{\text{ho}}(x)|^4 dx$ , whereas for the strongly interaction regime,  $E(\phi_k^\beta) \approx \frac{2}{3} \beta^{2/3}$ .

These observations are consistent with the results in [6, 7].

### 5.3.2. Numerical results in 2D

**Example 5.11.** In this example, we compute excited states in 2D BECs for the following four cases with various  $\beta$ .

- Case I.  $V(x, y) = V_{\text{box}}(x, y)$  (5.21),  $U = [0, 1]^2$ ;  
Case II.  $V(x, y) = V_{\text{ho}}(x, y)$  (5.22),  $U = [-10, 10]^2$ ;  
Case III.  $V(x, y) = V_{\text{hol}}(x, y)$  (5.23) with  $\kappa = 25$ ,  $U = [-10, 10]^2$ ;  
Case IV.  $V(x, y) = V_{\text{hol}}(x, y)$  (5.23) with  $\kappa = 50$ ,  $U = [-10, 10]^2$ .

As suggested by subsection 5.1, the information of initial guesses is given in Table 4. We compute the ground state (by the normalized gradient flow [5, 33]) and a few excited states for four cases

Table 4: Initial guesses in Example 5.11.  $\varphi_j = \phi_j^{\text{box}}$  (5.10) for Case I and  $\varphi_j = \phi_j^{\text{ho}}$  (5.11) for Cases II-IV.

solution	$k$ (index)	initial guess for $\phi$	initial guess for $(v_1, \dots, v_k)$
$\phi_g$	0	$\varphi_{(0,0)}$	–
$\phi_{10}$	1	$\varphi_{(1,0)}$	$\varphi_{(0,0)}$
$\phi_{01}$	1	$\varphi_{(0,1)}$	$\varphi_{(0,0)}$
$\phi_{10+01}$	1	$[\varphi_{(1,0)} + \varphi_{(0,1)}]/\sqrt{2}$	$\varphi_{(0,0)}$
$\phi_{10-01}$	1	$[\varphi_{(1,0)} - \varphi_{(0,1)}]/\sqrt{2}$	$\varphi_{(0,0)}$
$\phi_{11}$	3	$\varphi_{(1,1)}$	$(\varphi_{(0,0)}, \varphi_{(1,0)}, \varphi_{(0,1)})$

Table 5: Energies and chemical potentials of ground and excited states for Case I in Example 5.11.

$\beta$	$E_g$	$E_{10}$	$E_{01}$	$E_{10+01}$	$E_{10-01}$	$E_{11}$
0	9.8696	24.6740	24.6740	24.6740	24.6740	39.4784
10	19.4655	34.7611	34.7611	36.3205	36.3205	50.1222
50	49.2110	67.5593	67.5593	72.1768	72.1768	86.3251
100	81.8684	103.473	103.473	110.034	110.034	125.648
500	314.632	351.897	351.897	365.667	365.667	389.910
1000	589.286	638.718	638.718	657.680	657.680	688.933
$\beta$	$\mu_g$	$\mu_{10}$	$\mu_{01}$	$\mu_{10+01}$	$\mu_{10-01}$	$\mu_{11}$
0	9.8696	24.6740	24.6740	24.6740	24.6740	39.4784
10	28.0732	44.0760	44.0760	46.9070	46.9070	60.2603
50	83.3738	105.336	105.336	112.458	112.458	127.971
100	145.019	172.513	172.513	182.220	182.220	200.761
500	594.368	646.225	646.225	666.306	666.306	698.892
1000	1131.39	1201.69	1201.69	1229.47	1229.47	1272.81

Table 6: Energies and chemical potentials of ground and excited states for Case II in Example 5.11.

$\beta$	$E_g$	$E_{10}$	$E_{01}$	$E_{10+01}$	$E_{10-01}$	$E_{11}$
0	1.0000	2.0000	2.0000	2.0000	2.0000	3.0000
10	1.5923	2.4916	2.4916	2.4916	2.4916	3.4003
50	2.8960	3.7111	3.7111	3.7111	3.7111	4.5283
100	3.9459	4.7329	4.7329	4.7329	4.7329	5.5204
500	8.5118	9.2567	9.2567	9.2567	9.2567	10.0014
1000	11.9718	12.7059	12.7059	12.7059	12.7059	13.4399
$\beta$	$\mu_g$	$\mu_{10}$	$\mu_{01}$	$\mu_{10+01}$	$\mu_{10-01}$	$\mu_{11}$
0	1.0000	2.0000	2.0000	2.0000	2.0000	3.0000
10	2.0638	2.9094	2.9094	2.9094	2.9094	3.7618
50	4.1430	4.9128	4.9128	4.9128	4.9128	5.6813
100	5.7598	6.5109	6.5109	6.5109	6.5109	7.2613
500	12.6783	13.4051	13.4051	13.4051	13.4051	14.1317
1000	17.8886	18.6097	18.6097	18.6097	18.6097	19.3306

with various  $\beta = 0, 10, 50, 100, 500, 1000$ . Tables 5-8 list the energies and chemical potentials of these solutions. Fig. 7 plots the pseudo-color images of excited states with  $\beta = 1000$ .

From the numerical results shown in Fig. 7, Tables 5-8, and additional experimental results not shown here, we have the following numerical observations:

- (i) From Tables 5-8, we observe that for each case,  $E(\phi_{10}) = E(\phi_{01})$ ,  $\mu(\phi_{10}) = \mu(\phi_{01})$ ,  $E(\phi_{10+01}) = E(\phi_{10-01})$ , and  $\mu(\phi_{10+01}) = \mu(\phi_{10-01})$ . From Fig. 7, the profiles of  $\phi_{01}$  and  $\phi_{10-01}$  can be obtained from that of  $\phi_{10}$  and  $\phi_{10+01}$ , respectively, by a  $90^\circ$  rotation. Moreover, some boundary/interior layers and multiscale structures are observed. It is worthwhile to point out that, the shape and symmetry of excited states are independent of the shape of domain if  $V(\mathbf{x})$  is a harmonic or optical lattice potential and the computational domain is large enough so that the error of domain truncation can be ignored, whereas they are affected by the shape of domain if  $V(\mathbf{x})$  is a box potential.
- (ii) Tables 5-8 show the following facts:

Table 7: Energies and chemical potentials of ground and excited states for Case III in Example 5.11.

$\beta$	$E_g$	$E_{10}$	$E_{01}$	$E_{10+01}$	$E_{10-01}$	$E_{11}$
0	5.4894	10.8158	10.8158	10.8158	10.8158	16.1421
10	8.6291	13.0150	13.0150	12.8903	12.8903	17.9353
50	13.4615	16.4307	16.4307	15.4508	15.4508	20.1165
100	16.0172	18.7438	18.7438	17.5627	17.5627	21.6350
500	24.5175	26.3802	26.3802	25.6729	25.6729	28.2840
1000	29.8150	31.4142	31.4142	30.8570	30.8570	33.0400
$\beta$	$\mu_g$	$\mu_{10}$	$\mu_{01}$	$\mu_{10+01}$	$\mu_{10-01}$	$\mu_{11}$
0	5.4894	10.8158	10.8158	10.8158	10.8158	16.1421
10	11.0942	14.3353	14.3353	13.9468	13.9468	18.9615
50	16.7198	19.4602	19.4602	17.9147	17.9147	21.9572
100	20.2267	22.3176	22.3176	21.2398	21.2398	24.2538
500	31.2499	32.7361	32.7361	32.2639	32.2639	34.1864
1000	38.3834	39.6557	39.6557	39.2391	39.2391	41.0250

Table 8: Energies and chemical potentials of ground and excited states for Case IV in Example 5.11.

$\beta$	$E_g$	$E_{10}$	$E_{01}$	$E_{10+01}$	$E_{10-01}$	$E_{11}$
0	7.7626	15.3637	15.3637	15.3637	15.3637	22.9649
10	12.2495	17.1385	17.1385	16.6037	16.6037	23.7793
50	17.6091	21.4544	21.4544	19.8357	19.8357	25.6103
100	20.8412	24.1152	24.1152	22.6530	22.6530	27.4948
500	32.2079	34.6044	34.6044	33.8998	33.8998	37.0849
1000	39.6188	41.7623	41.7623	41.0769	41.0769	43.9528
$\beta$	$\mu_g$	$\mu_{10}$	$\mu_{01}$	$\mu_{10+01}$	$\mu_{10-01}$	$\mu_{11}$
0	7.7626	15.3637	15.3637	15.3637	15.3637	22.9649
10	15.7812	18.6102	18.6102	17.5856	17.5856	24.2988
50	21.7101	24.9488	24.9488	23.2633	23.2633	27.6786
100	25.9323	28.4524	28.4524	27.4443	27.4443	30.9539
500	41.7854	43.8228	43.8228	43.2263	43.2263	46.1402
1000	51.2663	52.9797	52.9797	52.3203	52.3203	54.7172

- For Case I with  $\beta > 0$ ,

$$E(\phi_g) < E(\phi_{10}) = E(\phi_{01}) < E(\phi_{10+01}) = E(\phi_{10-01}) < E(\phi_{11}),$$

$$\mu(\phi_g) < \mu(\phi_{10}) = \mu(\phi_{01}) < \mu(\phi_{10+01}) = \mu(\phi_{10-01}) < \mu(\phi_{11}).$$

- For Case II with  $\beta > 0$  (or each case with  $\beta = 0$ ),

$$E(\phi_g) < E(\phi_{10}) = E(\phi_{01}) = E(\phi_{10+01}) = E(\phi_{10-01}) < E(\phi_{11}),$$

$$\mu(\phi_g) < \mu(\phi_{10}) = \mu(\phi_{01}) = \mu(\phi_{10+01}) = \mu(\phi_{10-01}) < \mu(\phi_{11}).$$

- For Cases III and IV with  $\beta > 0$ ,

$$E(\phi_g) < E(\phi_{10+01}) = E(\phi_{10-01}) < E(\phi_{10}) = E(\phi_{01}) < E(\phi_{11}),$$

$$\mu(\phi_g) < \mu(\phi_{10+01}) = \mu(\phi_{10-01}) < \mu(\phi_{10}) = \mu(\phi_{01}) < \mu(\phi_{11}).$$

Consequently, for all cases in this example, the order of energies is consistent with that of chemical potentials of solutions we obtained. The first excited states are exactly index-1 excited states, but different index-1 excited states may have different energies and chemical potentials. Moreover, the index-3 excited state  $\phi_{11}$  possess higher energy and larger chemical potential than those of index-1 excited states.

These numerical results indicate that the Morse index of the excited state has a certain monotonous dependence on energy and chemical potential (i.e., the higher the index, the larger the energy and chemical potential), but generally there is no strict one-to-one correspondence.

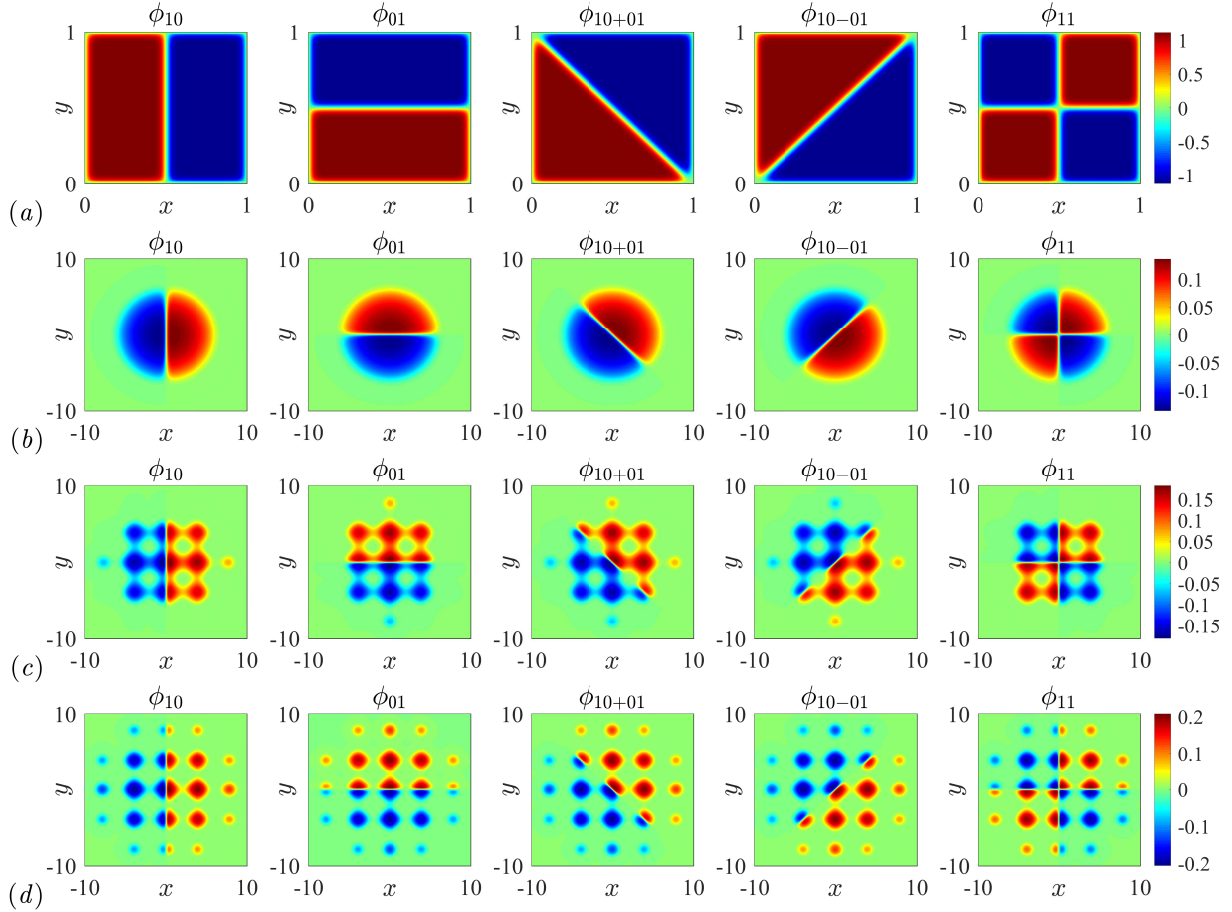


Figure 7: Four index-1 excited states  $\phi_{10}(x, y)$  (left column),  $\phi_{01}(x, y)$  (second column),  $\phi_{10+01}(x, y)$  (third column),  $\phi_{10-01}(x, y)$  (fourth column) and an index-3 excited state  $\phi_{11}(x, y)$  (right column) with  $\beta = 1000$  in Example 5.11. (a)  $\sim$  (d) for Cases I $\sim$ IV, respectively.

## 6. Concluding remarks

In this paper, a constrained gentlest ascent dynamics (CGAD) for finding general constrained saddle points with any specified Morse index was proposed. The linearly stable steady state of the CGAD was proved to be exactly a nondegenerate constrained saddle point with the corresponding index. The locally exponential convergence of an idealized CGAD around a nondegenerate constrained saddle point with the corresponding Morse index was also provided. Moreover, the CGAD was applied to compute some excited states of single-component Bose–Einstein condensates by finding constrained saddle points of the corresponding Gross–Pitaevskii energy functional under the normalization constraint. The properties of excited states were studied both mathematically and numerically. Extensive numerical results were reported to show the effectiveness and robustness of our method and demonstrate some interesting physics. It is worthwhile to point out that the CGAD can be applied to solve many other scientific problems. And, many optimization and preconditioning techniques can be used to further improve the computational efficiency of the CGAD. Some related works are ongoing.

## Acknowledgments

This work was supported by the NSFC grants 12101252, 12171148, 11971007, 11771138 and the innovation platform open fund of the Education Department in Hunan Province (18K025). The



work of W. Liu was also partially supported by the International Postdoctoral Exchange Fellowship Program No. PC2021024 and the Guangdong Basic and Applied Basic Research Foundation grant 2022A1515010351.

### Appendix A. Proof of Lemma 3.2

For  $l = 1, 2, \dots, m$  and  $i = 1, 2, \dots, k$ , applying (3.11) and noting that  $\langle G'_l(u), \hat{H}(u)v_i \rangle = 0$ , we have

$$\begin{aligned} \frac{d}{dt} \langle G'_l(u), v_i \rangle &= \langle G''_l(u)\dot{u}, v_i \rangle + \langle G'_l(u), \dot{v}_i \rangle \\ &= -\frac{1}{\gamma_0} \left\langle G''_l(u)v_i, F(u) - 2 \sum_{j=1}^k \langle F(u), v_j \rangle v_j \right\rangle \\ &\quad + \frac{1}{\gamma_i} \sum_{j=1}^i \lambda_{ij} \langle G'_l(u), v_j \rangle + \frac{1}{\gamma_i} \sum_{l'=1}^m \bar{\lambda}_{il'} \langle G'_l(u), G'_{l'}(u) \rangle. \end{aligned}$$

By the definition of  $\bar{\lambda}_{il'}$  in (3.13), which is equivalent to

$$-\frac{1}{\gamma_0} \left\langle G''_l(u)v_i, F(u) - 2 \sum_{j=1}^k \langle F(u), v_j \rangle v_j \right\rangle + \frac{1}{\gamma_i} \sum_{l'=1}^m \bar{\lambda}_{il'} \langle G'_l(u), G'_{l'}(u) \rangle = 0,$$

it holds,

$$\frac{d}{dt} \begin{pmatrix} \langle G'_l(u), v_1 \rangle \\ \langle G'_l(u), v_2 \rangle \\ \vdots \\ \langle G'_l(u), v_k \rangle \end{pmatrix} = \begin{pmatrix} \tilde{\lambda}_{11} & 0 & \cdots & 0 \\ \tilde{\lambda}_{21} & \tilde{\lambda}_{22} & \cdots & 0 \\ \vdots & \vdots & \ddots & \vdots \\ \tilde{\lambda}_{k1} & \tilde{\lambda}_{k2} & \cdots & \tilde{\lambda}_{kk} \end{pmatrix} \begin{pmatrix} \langle G'_l(u), v_1 \rangle \\ \langle G'_l(u), v_2 \rangle \\ \vdots \\ \langle G'_l(u), v_k \rangle \end{pmatrix}, \quad l = 1, 2, \dots, m,$$

with  $\tilde{\lambda}_{ij} := \lambda_{ij}/\gamma_i$  ( $1 \leq j \leq i \leq k$ ). Then the conclusion (3.15b) follows from the initial condition (3.14b). Moreover, by using (3.11) and (3.15b), and noting that  $\langle G'_l(u), F(u) \rangle = 0$ ,  $l = 1, 2, \dots, m$ , we have

$$\frac{d}{dt} G_l(u) = \langle G'_l(u), \dot{u} \rangle = \frac{2}{\gamma_0} \sum_{i=1}^k \langle F(u), v_i \rangle \langle G'_l(u), v_i \rangle = 0, \quad l = 1, 2, \dots, m.$$

Thus, (3.15a) is verified immediately from (3.14a). Furthermore, by using (3.11), (3.12) and (3.15b), we have, for  $1 \leq j \leq i \leq k$ ,

$$\begin{aligned} \frac{d}{dt} (\langle v_i, v_j \rangle - \delta_{ij}) &= \langle \dot{v}_i, v_j \rangle + \langle v_i, \dot{v}_j \rangle \\ &= -\left( \frac{1}{\gamma_i} + \frac{1}{\gamma_j} \right) \langle \hat{H}(u)v_i, v_j \rangle + \frac{1}{\gamma_i} \sum_{l=1}^i \lambda_{il} \langle v_l, v_j \rangle + \frac{1}{\gamma_j} \sum_{l=1}^j \lambda_{jl} \langle v_l, v_i \rangle \\ &= \begin{cases} \frac{2}{\gamma_i} \sum_{l=1}^i \lambda_{il} (\langle v_i, v_l \rangle - \delta_{il}), & j = i, \\ \frac{1}{\gamma_i} \sum_{l=1}^i \lambda_{il} (\langle v_l, v_j \rangle - \delta_{jl}) + \frac{1}{\gamma_j} \sum_{l=1}^j \lambda_{jl} (\langle v_l, v_i \rangle - \delta_{il}), & j < i. \end{cases} \end{aligned}$$

Denote  $\mathbf{y}$  as the vector of length  $\frac{k(k+1)}{2}$  formed by  $(\langle v_i, v_j \rangle - \delta_{ij}), 1 \leq j \leq i \leq k$ . Then, we have  $\mathbf{y}'(t) = \mathbf{A}(t)\mathbf{y}(t)$ , where  $\mathbf{A}$  is a matrix of degree  $\frac{k(k+1)}{2}$ , whose elements only depend on Lagrange multipliers  $\lambda_{ij}, 1 \leq j \leq i \leq k$  (3.12) and relaxation constants. The initial condition  $\mathbf{y}(0) = \mathbf{0}$  (3.14) leads to  $\mathbf{y}(t) \equiv \mathbf{0}$ . That is (3.15c). The proof is completed.

## Appendix B. Proof of Lemma 4.1

Note that, by (2.4),

$$\sum_{j=1}^m \langle G'_i(u), G'_j(u) \rangle \mu_j(u) = \langle G'_i(u), E'(u) \rangle, \quad i = 1, 2, \dots, m.$$

Differentiating in both sides of the above equation and applying the definitions of  $F(u)$  (2.4) and  $H(u)$ , we obtain

$$\begin{aligned} \sum_{j=1}^m \langle G'_i(u), G'_j(u) \rangle \mu'_j(u) &= G''_i(u)E'(u) + E''(u)G'_i(u) - \sum_{j=1}^m \mu_j(u) [G''_i(u)G'_j(u) + G''_j(u)G'_i(u)] \\ &= G''_i(u)F(u) + H(u)G'_i(u), \quad i = 1, 2, \dots, m. \end{aligned}$$

Thus

$$\mu'_i(u) = \sum_{j=1}^m g_{ij}(u) [G''_j(u)F(u) + H(u)G'_j(u)], \quad i = 1, 2, \dots, m.$$

For any  $v \in T_u\mathcal{M}$ , applying definitions of  $P_u$  (2.3) and  $\hat{H}(u)$  (2.5), yields

$$\begin{aligned} F'(u)v &= E''(u)v - \sum_{i=1}^m \mu_i(u)G''_i(u)v - \sum_{i=1}^m \langle \mu'_i(u), v \rangle G'_i(u) \\ &= H(u)v - \sum_{i=1}^m \sum_{j=1}^m g_{ij}(u) [\langle G''_j(u)F(u), v \rangle + \langle H(u)G'_j(u), v \rangle] G'_i(u) \\ &= \hat{H}(u)v - \sum_{i=1}^m \sum_{j=1}^m g_{ij}(u) \langle G''_j(u)F(u), v \rangle G'_i(u), \end{aligned}$$

where the self-adjointness of  $H(u)$  and the fact  $P_uv = v$  are used. The proof is completed.

## References

- [1] M. H. Anderson, J. R. Ensher, M. R. Matthews, C. E. Wieman, and E. A. Cornell. Observation of Bose-Einstein condensation in a dilute atomic vapor. *Science*, 269(5221):198–201, 1995.
- [2] X. Antoine, C. Besse, R. Duboscq, and V. Rispoli. Acceleration of the imaginary time method for spectrally computing the stationary states of Gross-Pitaevskii equations. *Comput. Phys. Commun.*, 219:70–78, 2017.
- [3] W. Bao and Y. Cai. Mathematical theory and numerical methods for Bose-Einstein condensation. *Kinet. Relat. Mod.*, 6(1):1–135, 2013.
- [4] W. Bao, I.-L. Chern, and F. Y. Lim. Efficient and spectrally accurate numerical methods for computing ground and first excited states in Bose-Einstein condensates. *J. Comput. Phys.*, 219(2):836–854, 2006.
- [5] W. Bao and Q. Du. Computing the ground state solution of Bose-Einstein condensates by a normalized gradient flow. *SIAM J. Sci. Comput.*, 25(5):1674–1697, 2004.
- [6] W. Bao and F. Y. Lim. Analysis and computation for the semiclassical limits of the ground and excited states of the Gross-Pitaevskii equation. *Proc. Sympos. Appl. Math., Amer. Math. Soc.*, 67:195–215, 2009.
- [7] W. Bao, F. Y. Lim, and Y. Zhang. Energy and chemical potential asymptotics for the ground state of Bose-Einstein condensates in the semiclassical regime. *Bull. Inst. Math. Acad. Sin. (N.S.)*, 2(2):495–532, 2007.
- [8] C. C. Bradley, C. A. Sackett, J. J. Tollett, and R. G. Hulet. Evidence of Bose-Einstein condensation in an atomic gas with attractive interactions. *Phys. Rev. Lett.*, 75:1687–1690, 1995.

- [9] K.-C. Chang. *Infinite Dimensional Morse Theory and Multiple Solution Problems*. Birkhäuser Boston, 1993.
- [10] S.-L. Chang and C.-S. Chien. Adaptive continuation algorithms for computing energy levels of rotating Bose-Einstein condensates. *Comput. Phys. Commun.*, 177(9):707–719, 2007.
- [11] C. Chen and Z. Xie. Search extension method for multiple solutions of a nonlinear problem. *Comput. Math. Appl.*, 47:327–343, 2004.
- [12] J.-H. Chen, I.-L. Chern, and W. Wang. Exploring ground states and excited states of spin-1 Bose-Einstein condensates by continuation methods. *J. Comput. Phys.*, 230(6):2222–2236, 2011.
- [13] Q. Cheng and J. Shen. Multiple scalar auxiliary variable (MSAV) approach and its application to the phase-field vesicle membrane model. *SIAM J. Sci. Comput.*, 40(6):A3982–A4006, 2018.
- [14] Y. S. Choi and P. J. McKenna. A mountain pass method for the numerical solution of semilinear elliptic problems. *Nonlinear Anal. Theor. Meth. Appl.*, 20(4):417–437, 1993.
- [15] F. Dalfovo, S. Giorgini, L. P. Pitaevskii, and S. Stringari. Theory of Bose-Einstein condensation in trapped gases. *Rev. Mod. Phys.*, 71:463–512, 1999.
- [16] K. B. Davis, M. O. Mewes, M. R. Andrews, N. J. van Druten, D. S. Durfee, D. M. Kurn, and W. Ketterle. Bose-Einstein condensation in a gas of sodium atoms. *Phys. Rev. Lett.*, 75:3969–3973, 1995.
- [17] Z. Ding, D. Costa, and G. Chen. A high-linking algorithm for sign-changing solutions of semilinear elliptic equations. *Nonlinear Anal.*, 38(2):151–172, 1999.
- [18] Q. Du, C. Liu, and X. Wang. A phase field approach in the numerical study of the elastic bending energy for vesicle membranes. *J. Comput. Phys.*, 198(2):450–468, 2004.
- [19] Q. Du and L. Zhang. A constrained string method and its numerical analysis. *Commun. Math. Sci.*, 7(4):1039–1051, 2009.
- [20] W. E, W. Ren, and E. Vanden-Eijnden. String method for the study of rare events. *Phys. Rev. B*, 66(5):052301, 2002.
- [21] W. E and X. Zhou. The gentlest ascent dynamics. *Nonlinearity*, 24(6):1831–1842, 2011.
- [22] W. Gao, J. Leng, and X. Zhou. Iterative minimization algorithm for efficient calculations of transition states. *J. Comput. Phys.*, 309:69–87, 2016.
- [23] D. Gilbarg and N. S. Trudinger. *Elliptic Partial Differential Equations of Second Order*. Springer, New York, 2001.
- [24] S. Gu and X. Zhou. Multiscale gentlest ascent dynamics for saddle point in effective dynamics of slow-fast system. *Commun. Math. Sci.*, 15:2279–2302, 2017.
- [25] S. Gu and X. Zhou. Convex splitting method for the calculation of transition states of energy functional. *J. Comput. Phys.*, 353:417–434, 2018.
- [26] G. Henkelman and H. Jónsson. A dimer method for finding saddle points on high dimensional potential surfaces using only first derivatives. *J. Chem. Phys.*, 111(15):7010–7022, 1999.
- [27] A. Levitt and C. Ortner. Convergence and cycling in walker-type saddle search algorithms. *SIAM J. Numer. Anal.*, 55(5):2204–2227, 2017.
- [28] C. Li, J. Lu, and W. Yang. Gentlest ascent dynamics for calculating first excited state and exploring energy landscape of Kohn-Sham density functionals. *J. Chem. Phys.*, 143(22):224110, 2015.
- [29] T. Li, P. Zhang, and W. Zhang. Nucleation rate calculation for the phase transition of diblock copolymers under stochastic Cahn-Hilliard dynamics. *Multiscale Model. Simul.*, 11(1):385–409, 2013.
- [30] Y. Li and J. Zhou. A minimax method for finding multiple critical points and its applications to semilinear PDEs. *SIAM J. Sci. Comput.*, 23(3):840–865, 2001.
- [31] Z. Li and J. Zhou. A local minimax method using virtual geometric objects: Part II-for finding equality constrained saddles. *J. Sci. Comput.*, 78:226–245, 2019.

- [32] E. H. Lieb and M. Loss. *Analysis*, volume 14 of *Graduate Studies in Mathematics*. Amer. Math. Soc., Providence, RI, 2nd edition, 2001.
- [33] W. Liu and Y. Cai. Normalized gradient flow with Lagrange multiplier for computing ground states of Bose-Einstein condensates. *SIAM J. Sci. Comput.*, 43(1):B219–B242, 2021.
- [34] D. Luenberger. *Optimization by Vector Space Methods*. Wiley, New York, 1969.
- [35] W. Quapp and J. M. Bofill. Locating saddle points of any index on potential energy surfaces by the generalized gentlest ascent dynamics. *Theor. Chem. Acc.*, 133:1510, 2014.
- [36] Ž. Marojević, E. Göklü, and C. Lämmerzahl. Energy eigenfunctions of the 1D Gross-Pitaevskii equation. *Comput. Phys. Commun.*, 184(8):1920–1930, 2013.
- [37] Z. Yang, Z. Li, and H. Zhu. Bifurcation method for solving multiple positive solutions to Henon equation. *Sci. China Ser. A Math.*, 51(12):2330–2342, 2008.
- [38] X. Yao. A Ljusternik-Schnirelman minimax algorithm for finding equality constrained saddle points and its application for solving eigen problems: part I. Algorithm and global convergence. *Adv. Comput. Math.*, 45:269–310, 2019.
- [39] X. Yao and J. Zhou. Numerical methods for computing nonlinear eigenpairs: Part I. Iso-homogeneous cases. *SIAM J. Sci. Comput.*, 29(4):1355–1374, 2007.
- [40] X. Yao and J. Zhou. Numerical methods for computing nonlinear eigenpairs: Part II. Non-iso-homogeneous cases. *SIAM J. Sci. Comput.*, 30(2):937–956, 2008.
- [41] J. Yin, L. Zhang, and P. Zhang. High-index optimization-based shrinking dimer method for finding high-index saddle points. *SIAM J. Sci. Comput.*, 41(6):A3576–A3595, 2019.
- [42] E. Zeidler. *Nonlinear Functional Analysis and its Applications III: Variational Methods and Optimization*. Springer-Verlag, New York, 1985.
- [43] J. Zhang and Q. Du. Constrained shrinking dimer dynamics for saddle point search with constraints. *J. Comput. Phys.*, 231(14):4745–4758, 2012.
- [44] J. Zhang and Q. Du. Shrinking dimer dynamics and its applications to saddle point search. *SIAM J. Numer. Anal.*, 50(4):1899–1921, 2012.
- [45] L. Zhang, W. Ren, A. Samanta, and Q. Du. Recent developments in computational modelling of nucleation in phase transformations. *npj Comput. Mater.*, 2:16003, 2016.